Investigating the Effect of Snow-Ice Formation on Snow Depth and Density over Arctic Sea Ice

Ioanna Merkouriadi[1], Glen Liston[2], Arttu Jutila[1], Heidi Sallila[3], and Andreas Preußer[4]

[1]Finnish Meteorological Institute
[2]Colorado State University
[3]FMI
[4]Alfred Wegener Institute, Helmholtz Centre for Polar and Marine Research

December 27, 2023

Abstract

We examined the effect of snow-ice formation on SnowModel-LG snow depth and density products. We coupled SnowModel-LG, a modeling system adapted for snow depth and density reconstruction over sea ice, with HIGHTSI, a 1-D thermodynamic sea ice model, to create SnowModel-LG_HS. Pan-Arctic model simulations spanned from 1 August 1980 through 31 July 2022. In SnowModel-LG_HS, domain average snow depth decreased by 20%, and snow density increased by 2% when compared to SnowModel-LG, with largest differences in the Atlantic sector. Averaged across the CryoSat-2 era (2011–2022), domain average April sea ice thickness retrievals from CryoSat-2 decreased by 7.7% when snow-ice was accounted for. Evaluation of SnowModel-LG HS against snow depth, snow-ice, and sea ice thickness observations highlighted the importance of snow redistribution over deformed sea ice. The findings suggest that neglecting snow and sea ice interactions in models can lead to substantial overestimation of snow depth over level ice.

Investigating the Effect of Snow-Ice Formation on Snow Depth and Density over Arctic Sea Ice

I. Merkouriadi[1], G. E. Liston[2], A. Jutila[1], H. Sallila[1], A. Preußer[3]

[1]Finnish Meteorological Institute, Helsinki, Finland
[2]Cooperative Institute for Research in the Atmosphere, Colorado State University, Fort Collins, CO, USA
[3]Alfred-Wegener-Institut, Helmholtz-Zentrum für Polar- und Meeresforschung, Bremerhaven, Germany

Key Points:

- We examined the changes in modeled snow depth and density over sea ice caused by snow-ice formation.
- Accounting for snow and sea ice interactions markedly reduces snow depth on level ice.
- Sea ice thickness retrievals from radar altimetry change on average by 7.7 % when snow products account for snow-ice.

Corresponding author: Ioanna Merkouriadi, `ioanna.merkouriadi@fmi.fi`

Abstract

We examined the effect of snow-ice formation on SnowModel-LG snow depth and density products. We coupled SnowModel-LG, a modeling system adapted for snow depth and density reconstruction over sea ice, with HIGHTSI, a 1-D thermodynamic sea ice model, to create SnowModel-LG_HS. Pan-Arctic model simulations spanned from 1 August 1980 through 31 July 2022. In SnowModel-LG_HS, domain average snow depth decreased by 20 %, and snow density increased by 2 % when compared to SnowModel-LG, with largest differences in the Atlantic sector. Averaged across the CryoSat-2 era (2011–2022), domain average April sea ice thickness retrievals from CryoSat-2 decreased by 7.7 % when snow-ice was accounted for. Evaluation of SnowModel-LG_HS against snow depth, snow-ice, and sea ice thickness observations highlighted the importance of snow redistribution over deformed sea ice. The findings suggest that neglecting snow and sea ice interactions in models can lead to substantial overestimation of snow depth over level ice.

Plain Language Summary

The amount of snow on sea ice is important for monitoring sea ice thickness, which is one of the key factors in a changing climate. Recent advances in snow-on-sea-ice modeling have made it possible to simulate snow depth and density over Arctic sea ice. However, these simulations often do not consider how much snow is lost to snow and sea ice interactions, such as snow-ice formation. Snow-ice forms when snow becomes part of the sea ice, after seawater floods the sea ice surface and freezes inside the snow. In this study, we combined a snow model with a sea ice model to understand how snow changes when snow-ice forms. Our results show that when snow-ice forms, snow depth decreases, and snow density commonly increases. The differences are highest in the Atlantic sector of the Arctic, where snow-ice is more likely to form due to high annual snowfall.

1 Introduction

Arctic sea ice is going through unprecedented changes, decreasing dramatically both in extent (e.g. Stroeve et al., 2014) and in thickness (Kwok et al., 2009; Maslanik et al., 2007), and transitioning from a multiyear ice to a seasonal, first-year ice system (Meier et al., 2014). The role of snow cover over thinner, seasonal sea ice is amplified in many ways. First, the thermal resistance of snow cover becomes a dominant control over the atmosphere-ocean heat fluxes, regulating sea ice growth in winter. Second, the snow load becomes more likely to submerge thinner ice underneath the water level, creating negative freeboard conditions. If sea water floods at the ice/snow interface and freezes there, snow-ice is formed, that is a mixture of frozen seawater and snow (e.g. Leppäranta, 1983). Snow-ice is a common phenomenon in seas that are seasonally covered by ice (i.e., Baltic Sea, Sea of Okhotsk), but it was not commonly observed in drifting Arctic sea ice until the Norwegian Young Sea ICE (N-ICE2015) expedition (Granskog et al., 2017; Provost et al., 2017). Snow-ice is a sink for snow, and it can contribute significantly to the sea ice mass balance (Merkouriadi et al., 2017, 2020). Therefore, it is essential to consider it for improving Arctic sea ice forecasts.

Satellite altimetry is the most common method for monitoring sea ice thickness, providing nearly full coverage of the Arctic Ocean (Landy et al., 2022; Laxon et al., 2003; Markus et al., 2017). Information on the snow load exerted on sea ice is crucial for altimetry retrievals of sea ice thickness, because radar and laser altimeters, in principle, measure ice or snow freeboard; the elevation of the ice or snow surface from the water surface. Snow depth and density are required to convert freeboard to sea ice thickness information (e.g. Kurtz et al., 2009). According to Giles et al. (2007), uncertainties in snow depth and density contribute 48 % and 14 %, respectively, to the total error of sea ice thickness retrievals from radar altimetry. A more recent study by Landy et al. (2020)

estimated these uncertainties at 11 % for snow depth and 16 % for density. Similarly, snow depth and density uncertainties were found to contribute 70 % and 30–35 %, respectively, to the total error of sea ice thickness retrievals from laser altimetry (Zygmuntowska et al., 2014).

Snow depth and density estimates used in altimetry applications are often derived from snow climatologies or their modified versions. The most widely used snow-on-sea-ice climatology is compiled from a snow depth and density data set collected decades ago mostly over multiyear ice (Warren et al., 1999). In a changing Arctic sea ice system, snow conditions are expected to change as well (Blanchard-Wrigglesworth et al., 2015; Webster et al., 2014), and these changes are not captured by the Warren et al. (1999) climatology. In addition to the long-term changes, climatology overlooks the spatio-temporal differences and interannual variability of snow conditions in the Arctic, which are evidently strong (Webster et al., 2019). Addressing the imperative need for better representation of snow on sea ice, efforts have focused on reanalysis-based snow depth and density reconstructions (e.g. Blanchard-Wrigglesworth et al., 2018; Kwok & Cunningham, 2008; Petty et al., 2018). A recent contribution was SnowModel-LG, a state-of-the-art Lagrangian snow evolution model (Liston, Itkin, et al., 2020). Compared to other reanalysis-based products, SnowModel-LG implemented higher resolution Lagrangian parcel tracking and included an improved representation of snow evolution physics. It has been bias-corrected and validated against a wide observation framework, and yielded good agreement, especially with in situ measurements (Stroeve et al., 2020). However, neither SnowModel-LG nor any of the above-mentioned snow products account for snow losses due to snow and sea ice interactions, such as snow-ice formation.

This study aims to examine snow loss through snow-ice formation, and its effect in SnowModel-LG snow depth and density simulations over the Arctic Ocean, from 1 August 1980 through 31 July 2022. To investigate this, we coupled SnowModel-LG with the High-Resolution Thermodynamic Sea Ice model (HIGHTSI) (Launiainen & Cheng, 1998) to produce SnowModel-LG_HS. In HIGHTSI, snow-ice forms when the sea ice surface is depressed below the water surface (negative freeboard), with the assumption that all negative freeboard will result in flooding and, consequently, snow-ice formation. We investigated the effect of both snow depth and density products (SnowModel-LG and SnowModel-LG_HS) on sea ice thickness retrievals from satellite radar altimetry (CryoSat-2). We discuss the results in light of an evaluation exercise we performed using observations from airborne campaigns and drifting ice mass balance buoys (IMBs).

2 Materials and Methods

2.1 SnowModel-LG

SnowModel is a collection of snow distribution and snow evolution modeling tools, applicable to any environment experiencing snow, including sea ice applications (Liston & Elder, 2006a). SnowModel-LG is adapted for snow depth and density reconstruction over sea ice (Liston, Itkin, et al., 2020). It is implemented in a Lagrangian framework to simulate snow properties on drifting sea ice. SnowModel-LG accounts for physical snow processes such as sublimation from static surfaces and blowing snow, snow melt, evolution of snow density and temperature profiles, energy and mass transfers within the snowpack, and superimposed ice formation in a multi-layer configuration.

At each time step (3-hour here), SnowModel-LG performs a mass-budget calculation, where snow water equivalent (SWE) depth (m) is defined by snow mass gains, losses, and ice parcel dynamics,

$$\frac{\mathrm{d}SWE}{\mathrm{d}t} = \frac{1}{\rho_w}\left[(P_r + P_s) - (S_{ss} + S_{bs} + M) + D\right] \tag{1}$$

where t (s) is time; $\rho_w = 1{,}000\,\mathrm{kg\,m^{-3}}$ is the water density; P_r ($\mathrm{kg\,m^{-2}\,s^{-1}}$) and P_s ($\mathrm{kg\,m^{-2}\,s^{-1}}$) are the water-equivalent rainfall and snowfall fluxes, respectively; S_{ss} ($\mathrm{kg\,m^{-2}\,s^{-1}}$) and S_{bs} ($\mathrm{kg\,m^{-2}\,s^{-1}}$) are the water-equivalent sublimation from static-surface and blowing-snow processes, respectively; M ($\mathrm{kg\,m^{-2}\,s^{-1}}$) is melt-related mass losses; and D ($\mathrm{kg\,m^{-2}\,s^{-1}}$) is mass losses and gains from sea ice dynamics processes (i.e., parcels being created and lost with ice motion, divergence, and convergence).

Snow depth h_s (m) is related to SWE through the ratio of snow (ρ_s), and water (ρ_w) densities,

$$SWE = \frac{\rho_s}{\rho_w} h_s. \tag{2}$$

Therefore, the evolution of snow depths and densities are calculated by

$$\frac{\mathrm{d}\left(\rho_s h_s\right)}{\mathrm{d}t} = \left(P_r + P_s\right) - \left(S_{ss} + S_{bs} + M\right) + D. \tag{3}$$

In SnowModel-LG, snow density evolves and changes in response to compaction (weight of the above snow layers), wind force, freezing of liquid water, and vapor flux through the snowpack. Additional information on the components and the configuration of SnowModel-LG are provided in detail in Liston, Itkin, et al. (2020). The model configuration in this study is identical to the one used in Liston, Itkin, et al. (2020), only here we have extended the simulation for another four years. According to Stroeve et al. (2020), SnowModel-LG performed well in capturing the spatial and seasonal variation of snow distributions, when evaluated against several Arctic data sets.

In the simulations presented herein, Lagrangian parcel tracking began on 1 August 1980. The first simulation year assumes no snow atop the sea ice; the following years carry available snow from 31 July to 1 August. Essential inputs are atmospheric reanalysis estimates of near-surface air temperature, relative humidity, precipitation, wind speed and direction, and sea ice motion and concentration products.

2.2 HIGHTSI

HIGHTSI is a 1-D thermodynamic sea ice model designed to simulate the evolution of snow and sea ice thickness and temperature profiles (Launiainen & Cheng, 1998) by solving the heat conduction equation for multiple ice and snow layers. The sea ice thermal conductivity is parameterized following Pringle et al. (2007). HIGHTSI simulates snow-ice formation following Saloranta (2000).

HIGHTSI has been widely used in process studies and validated extensively against observations (Cheng, Zhang, et al., 2008; Cheng et al., 2013; Merkouriadi et al., 2017, 2020; Wang et al., 2015). In this study, we used a model configuration that is derived from validation studies on Arctic sea ice. The model's vertical resolution has been found to be critical for its performance in the Arctic (Cheng, Vihma, et al., 2008). Here, we used 20 layers in the ice which is considered optimal for capturing internal thermodynamic processes (Cheng, Vihma, et al., 2008; Cheng, Zhang, et al., 2008; Cheng et al., 2013; Wang et al., 2015). Detailed information on model parameterizations is given in Table S1 in the supporting information (Briegleb et al., 2004; Cheng, Vihma, et al., 2008; Granskog et al., 2017; Grenfell & Maykut, 1977; Liston, Itkin, et al., 2020; Maykut & Untersteiner, 1971; Perovich, 1996; Pringle et al., 2007; Wang et al., 2015; Zuo et al., 2019).

Merkouriadi et al. (2020) implemented HIGHTSI in a Lagrangian framework to examine pan-Arctic snow-ice distributions. In the study presented herein, HIGHTSI was modified further, so that snow depth and density evolution were simulated by SnowModel-LG in a 25-layer configuration.

2.3 SnowModel-LG_HS

We performed two separate snow-on-sea-ice simulations. First, we simulated snow depth and density with SnowModel-LG (i.e. Liston, Itkin, et al., 2020). Second, SnowModel-LG's snow depth and density evolution were coupled with HIGHTSI's snow-ice and thermodynamic ice growth representations. The coupled modeling products are hereafter referred to as being created by SnowModel-LG_HS.

For the SnowModel-LG_HS runs, snow density was simulated following Appendix C of Liston, Itkin, et al. (2020), with the vertical density profile parameterized as being a linear fit between densities that are 20 % greater than the mean at the top of the snowpack (assumed to be wind slab), and 20 % less at the bottom of the snowpack (assumed to be depth hoar). These percentages are consistent with snow-pit measurements made during the Multidisciplinary drifting Observatory for the Study of Arctic Climate (MOSAiC) expedition (Macfarlane et al., 2023). This approach was chosen to provide a best-possible fit to available snow density observations, as opposed to relying completely on SnowModel-LG's representation of the vertical density evolution. To account for changes in snow density in response to snow-ice formation, when snow-ice was formed, the corresponding snow-depth amount was removed from the bottom layers of the snowpack, and the bulk density was recalculated based on the depth and density of the remaining snow. Additional model specifications are presented in the supporting information (Table S1).

2.4 Input Data Sets

Daily ice concentrations (15–100 %) by DiGirolamo et al. (2022) were used to define whether an ice parcel existed and whether snow could accumulate on that parcel. Ice motion vectors from the National Snow and Ice Data Center (NSIDC) (Tschudi et al., 2019, 2020) gridded over 25-km spatial resolution were used as Lagrangian ice parcel tracks. NASA's Modern Era Retrospective Analysis for Research and Application Version 2 (MERRA-2; Gelaro et al., 2017; Global Modeling And Assimilation Office (GMAO), 2015a, 2015b) was used as atmospheric forcing to SnowModel-LG_HS. Specifically, SnowModel-LG_HS was forced with 10-m wind speed and direction, 2-m air temperature and relative humidity, and total water-equivalent precipitation from MERRA-2. During these simulations, MicroMet (Liston & Elder, 2006b) provided the required liquid and solid precipitation, and the downwelling shortwave and longwave radiation following Liston, Itkin, et al. (2020).

We applied the same bias-correction in MERRA-2 reanalysis as in Liston, Itkin, et al. (2020), where observations from NASA Operation IceBridge (OIB; 2009–2016) were used to scale the precipitation inputs. In Liston, Itkin, et al. (2020), 8-year averages of precipitation scaling factors were calculated and they were applied over all ice parcels and through the whole simulation period, making the results of MERRA-2 and the European Centre for Medium-Range Weather Forecasts (ECMWF) ReAnalysis-5th Generation (ERA5; Hersbach et al., 2020) model runs similar. Scaling factors were 1.37 for MERRA-2 and 1.58 for ERA5, indicating the need to increase the precipitation inputs in order to match the OIB observations. The same scaling factors were used in this study for the results to be comparable with the publicly available SnowModel-LG snow depth and density data set (Liston, Stroeve, & Itkin, 2020).

For the ocean boundary forcing, at the ice/ocean interface, we used ocean heat flux from the Ocean Reanalysis System 5 (ORAS5) provided at the ECMWF (Zuo et al., 2019). ORAS5 resolution is eddy-permitting (0.25° latitude and longitude) horizontally and 1 m vertically. ORAS5 includes five ensemble members and covers the period from 1979 onward. In our study, we used the ensemble mean, providing one unique value on a 1° grid for each simulation day.

2.5 Model Configuration and Outputs

The simulations began on 1 August 1980 and ran through 31 July 2022. Temporal resolution was 3 h to capture diurnal variations, and the parcel-specific outputs (e.g. snow depth, snow density, and snow-ice thickness) were saved at the end of each day. Ice parcel trajectories were linearly interpolated from weekly to 3-hourly time steps. On 1 August of each year (except in the first year), the multi-year ice thicknesses were calculated from the sea ice thickness distribution on 31 July. The 1 August 1980 ice thickness initial condition was defined by performing a one-year simulation with a domain-wide initial condition of 1 m, and then using the ice thickness distribution at the end of the first simulation year as the initial condition for the beginning of the 42-year simulation (i.e., the model ran the first year twice and assumed the 31 July 1981 ice thickness distribution equaled the 1 August 1980 distribution). In addition, any snow remaining at 00:00 UTC on 1 August (the last time step on 31 July) was used as the initial condition for the following simulation year that started at 03:00 UTC on 1 August (these are the standard procedures implemented in Liston, Itkin, et al. (2020)).

The daily simulation outputs for each parcel (approximately 61,000 parcels each year) were gridded to the 25 km × 25 km Equal-Area Scalable Earth (EASE) grid, provided by NSIDC. The location of each parcel was used to calculate the overlap between that parcel and the EASE grid cell, i.e. the fractional area of the EASE grid cell that was occupied by the parcel. The fractional area was then multiplied by the sea ice concentration of the parcel, and the result was used to weigh the parcels' contribution to each EASE grid cell. This procedure of area- and concentration-weighted averages within the EASE grid cells conserved the examined parameters, similar to Merkouriadi et al. (2020).

2.6 Altimetry Applications

To study the impact of snow-ice formation in a wider context, we tested the SnowModel-LG_HS snow estimates in sea ice thickness retrievals from satellite altimetry. From the European Space Agency's (ESA) CryoSat-2 satellite, we processed Baseline-D (Baseline-E for winter 2021–2022) Level 1B Synthetic Aperture Radar (SAR) and SAR Interferometric files (European Space Agency, 2019a, 2019b, 2019c, 2019d) for the full winter season (September to May), starting in November 2010 and continuing through May 2022, using the python library pysiral (Hendricks et al., 2021). For the necessary auxiliary data in the sea ice thickness retrieval, we used the mean dynamic topography product by the Danish Technical University (DTU22MDT; Knudsen et al., 2022); for sea ice concentration and type, we used the European Organisation for the Exploitation of Meteorological Satellites (EUMETSAT) Ocean and Sea Ice Satellite Application Facility (OSI SAF) products 401-b and 403-d, respectively (OSI SAF, 2017a, 2017b).

The SnowModel-LG and SnowModel-LG_HS snow depths and densities were applied to preprocessed Level 1B files, and the processor was run first to produce Level 2 (along-track) and then to grid those to Level 3 (monthly gridded) files. For this study, we used the monthly gridded files.

2.7 Evaluation Exercise

To evaluate modeled snow depth and sea ice thickness, we compared them against independent airborne data from NASA OIB and Alfred Wegener Institute's (AWI) IceBird campaigns conducted during late-winter over the western Arctic. Snow depth data were derived from airborne snow radars similar on both OIB (99 flights in 2009–2019; Kurtz et al., 2015, 2016; MacGregor et al., 2021) and IceBird campaigns (11 flights in 2017 & 2019; Jutila et al., 2021a, 2021b; Jutila, King, et al., 2022), whereas sea ice thickness could be simultaneously and independently observed only on IceBird with a towed electromagnetic sounding instrument (Jutila et al., 2021a, 2021b; Jutila, Hendricks, et al., 2022). We averaged the airborne measurements over the same EASE grid when more than 50 values were present in a grid cell. For sea ice thickness, we included only level ice measurements using the flag in the data product that implements a total thickness gradient threshold of 4 cm within an along-track distance of 1 m.

In addition, we evaluated temperature profile and heating cycle data from thermistor strings of Snow Ice Mass Balance Apparatus (SIMBA) buoys (Jackson et al., 2013) deployed in the Arctic in 2012–2020 to detect flooding (Grosfeld et al., 2016; Lei et al., 2021, 2022, 2023). Changes in thermal diffusivity, temperature, and heat propagation distinguish the temporal evolution of different layers and their thicknesses (e.g. Provost et al., 2017).

3 Results

In this section, we present two snow depth and density products. The first product is based on the original SnowModel-LG model, without accounting for snow-ice formation. We refer to it as SMLG. SMLG is identical to the one described in Liston, Itkin, et al. (2020), only here the SnowModel-LG run was extended for four more years (1 August 1980 to 31 July 2022). The second product accounts for snow-ice formation through the coupling of SnowModel-LG with HIGHTSI (SnowModel-LG_HS). We refer to this simulation as SMLG_HS. In what follows, we compare snow depth and density derived by the two different products, and we use both to retrieve sea ice thickness from CryoSat-2.

The model results indicated that snow-ice has the potential to form every year in the Arctic Ocean, and it is characterized by strong seasonal and regional variations. The seasonality and long-term trends of snow-ice thickness calculated in this study were consistent with earlier findings (Merkouriadi et al., 2020), as expected. The seasonal and interannual evolution of all simulated parameters is presented in Figure S1. Our coupled SMLG_HS simulation presented herein investigated the impact of snow-ice formation on snow depth and density (Figures 1a–c and d–f, respectively). Snow-ice formation occurred throughout the 42-year simulation period (1980–2022), and it was more prominent in the Atlantic sector of the Arctic Ocean, north of Svalbard, across the east coast of Greenland, and over the Lincoln Sea. Here, we show results averaged across the 42-year period on the day of maximum snow-on-sea-ice volume.

The date of maximum snow-on-sea-ice volume occurred on average on 21 April with a standard deviation of 14 d. There was no significant long-term trend of that date across the simulation period. The snow depth and density differences (SMLG_HS minus SMLG) were calculated on the date of maximum snow volume and averaged over the 42-year period (e.g., Figures 1c and f). Across the Arctic Ocean, accounting for snow-ice formation produced a 20 % snow depth decrease and a 2 % snow density increase, corresponding to 4 cm of snow depth and 6.6 $\mathrm{kg\,m^{-3}}$ of snow density. Regional variations were strong, yielding over 85 cm decrease in snow depth, and 209 $\mathrm{kg\,m^{-3}}$ increase in snow density, when compared to the original SMLG product.

Sea ice thickness retrievals from CryoSat-2 were performed using both SMLG and SMLG_HS. Averaged results from April are plotted together with the differences in sea ice thickness in Figure 1g–i. SMLG_HS represents less snow load on sea ice, resulting in thinner sea ice thickness retrievals by 7.7 % (domain average) across the CryoSat-2 era (2011–2022). Even though there are regional and inter-annual variations, the differences were more prominent in the Atlantic sector of the Arctic Ocean and over the Lincoln Sea (Figure 1g–i), i.e. in regions that are more prone to snow-ice formation (Merkouriadi et al., 2020). The differences regionally exceed 1 m in April, highlighting the sensitivity of the altimetry retrievals to snow load.

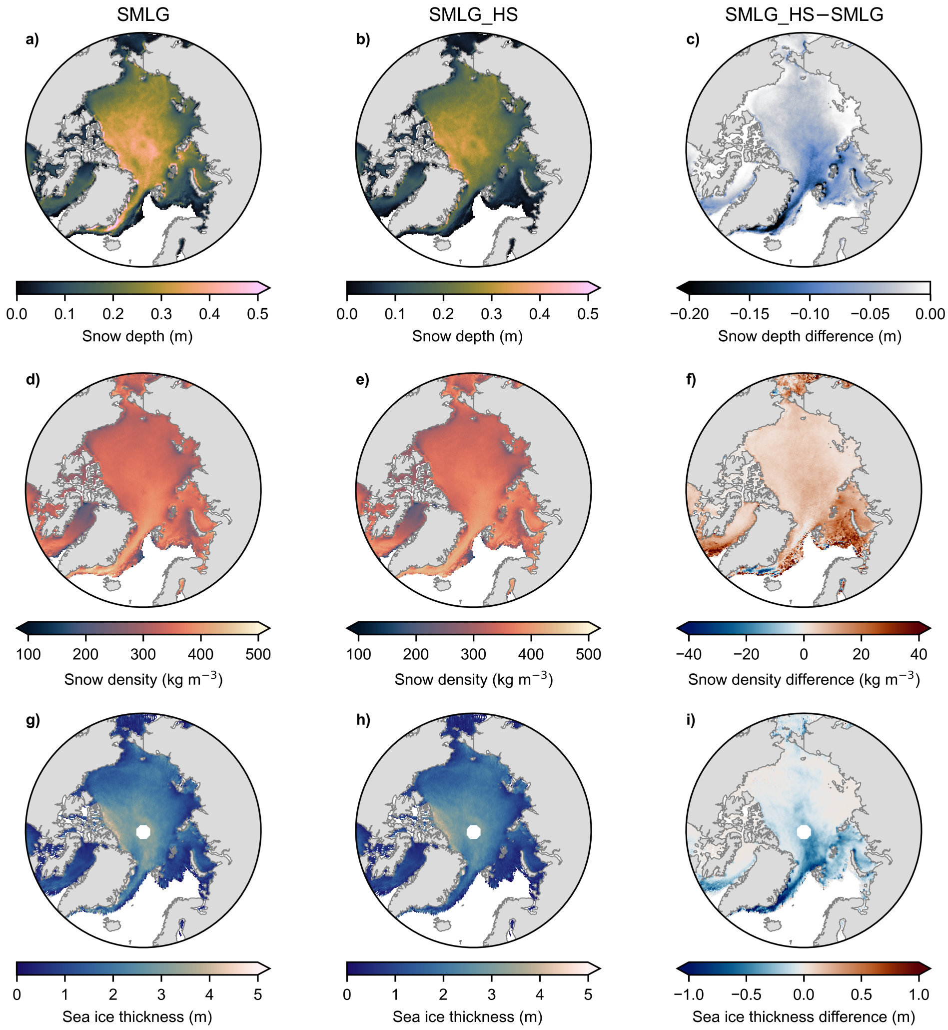

Figure 1. Snow depth (top) and snow density (middle) on the day of maximum snow-on-sea-ice volume (42-year average) as well as sea ice thickness (bottom) based on CryoSat-2 retrievals in April 2011–2022 from (a, d, g) SMLG, (b, e, h) SMLG_HS, and (c, f, i) the difference between the two products (SMLG_HS minus SMLG).

4 Discussion and Conclusions

We investigated the effect of snow-ice formation in snow depth and density reconstructions over Arctic sea ice in a modeling study. We did this by coupling SnowModel-LG snow depth and density evolution with HIGHTSI thermodynamic sea ice and snow-ice growth. When snow-ice was accounted for, snow depth decreased markedly and, in most cases, snow density increased. Averaged across the entire Arctic Ocean on the day of maximum snow-on-sea-ice volume, and for the period 1980–2022, snow depth given by SMLG_HS was 20 % lower than SMLG, and snow density was 2 % higher, corresponding to 4 cm of snow depth and 6.6 kg m^{-3} of snow density. Due to the large regional variations of snow-ice formation, snow depth decreased over 85 cm and density increased over 209 kg m^{-3} locally. The largest differences were found in the Atlantic sector of the Arctic Ocean, where snow-ice has the highest potential to form (Merkouriadi et al., 2020).

Largest differences in altimetry-derived sea ice thickness were found in the Atlantic sector and the Lincoln Sea, and they were consistent with the snow-ice contribution. In some years, the differences were notable in the central Arctic as well. Domain average sea ice thicknesses for the CryoSat-2 in April 2011–2022 were 7.7 % lower when using SMLG_HS compared to SMLG. It is worth mentioning that the effect of snow salinity on the altimetry signals becomes relevant when seawater floods the bottom of the snowpack (Willatt et al., 2010). SMLG_HS does not yet handle snow salinity and wicking in response to seawater flooding at the snow/ice interface. In addition to this, there is no temperature dependency in snow-ice formation in SMLG_HS. The model assumes that flooding — or negative freeboard — at the snow/ice interface corresponds to snow-ice formation in winter.

Due to the lack of information regarding several aspects of snow on sea ice, this study comes with some limitations. First, we assumed that a negative freeboard always results in snow-ice formation. In reality, for flooding to occur, water pathways such as sea ice thermal cracks or leads are required. Even though these pathways become increasingly common in a thinner and more dynamic icescape (Kwok et al., 2013; Rampal et al., 2009), our assumption likely resulted in overestimation of snow-ice formation. Second, we did not account for snow blowing into leads. Recent observations from the MOSAiC expedition demonstrated that this is likely an insignificant snow sink in winter, due to quick refreeze of the leads (Clemens-Sewall et al., 2023). This is further supported by the arguments put forth by Liston, Itkin, et al. (2020). Third, we assumed that snow accumulates on level ice, and we did not account for snow redistribution over deformed ice. Sea ice deformation features such as pressure ridges, are prominent in the Arctic Ocean, especially under a thinner and more dynamic sea ice regime (Itkin et al., 2017; Rampal et al., 2009). Snow tends to accumulate on the lee side of pressure ridges and other roughness elements (e.g. Liston et al., 2018), resulting in uneven snow load over a sea ice floe.

SMLG_HS snow depth fit well to both OIB and IceBird observations (Figures 2a–d), with reduced root-mean-square-errors and biases compared to SMLG (Figure S2). However, SMLG_HS constantly underestimated sea ice thickness of level ice, when compared to IceBird observations (Figures 2e–h and S3). We hypothesize that the sea ice thickness underestimation resulted from overestimation of the snow accumulation over level ice. Even though the total snow depth (over both deformed and level ice) matched well with the observations, not accounting for snow redistribution over deformed ice resulted in overestimation of snow depth over level ice. This additional snow decelerated thermodynamic ice growth, resulting in thinner sea ice that was more prone to snow-ice formation. Mid-winter flooding events at the snow/ice interface detected by IMBs supported our simulations of snow-ice formation (Figure S4). However, IMBs are point measurements and do not necessarily reflect the situation over larger spatial domains.

Although snow depth, and the associated snow-ice formation, have decreased Arctic-wide, modeling studies have indicated increasing trends in snow depth (Webster et al.,

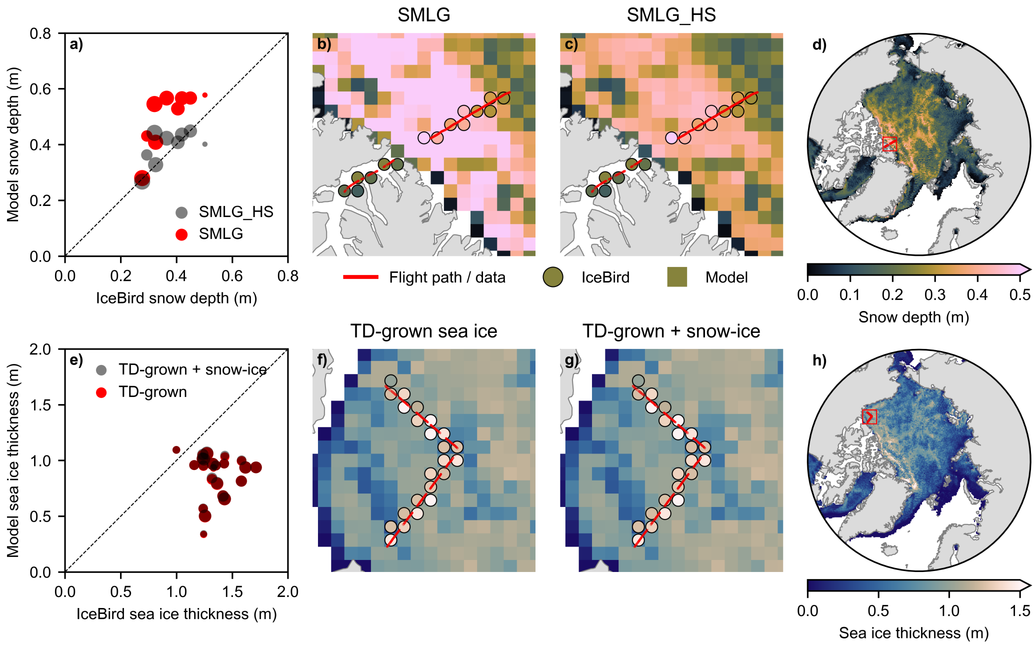

Figure 2. Panels a)–d) show the evaluation of modeled snow depth from SMLG and SMLG_HS against airborne radar-derived snow depth measurements from the AWI IceBird survey flight on 30 March 2017. Panels e)–h) show the evaluation of thermodynamically-grown (TD-grown) sea ice and snow-ice modeled with SMLG_HS against airborne sea ice thickness measurements over level ice from the AWI IceBird survey flight on 2 April 2017.

2019) and snow-ice (Merkouriadi et al., 2020) regionally in the Atlantic sector of the Arctic Ocean, especially along the east coast of Greenland, north of Svalbard, and at the Lincoln Sea since the 1980s. The increase is significant and it is associated with the intensification of storms that bring more precipitation to this part of the Arctic (Graham et al., 2017; Rinke et al., 2017; Woods & Caballero, 2016). When snow models do not account for snow sinks caused by snow and sea ice interactions, such as snow-ice formation or snow redistribution over sea ice deformation features, they overestimate snow depth on level ice. Uneven snow-on-sea-ice load within a sub-grid area will result in biases in altimetry retrievals of sea ice thickness by overestimating level ice and underestimating deformed ice thickness. Regarding sea ice modeling applications, spatial variability in snow depth will impact sea ice thermodynamic growth in winter and will affect meltpond formation in summer. Therefore, snow-on-sea-ice reconstructions should be used with caution depending on the application requirements. This study emphasizes the need to account for snow and sea ice interactions to improve the representation of snow on sea ice in both numerical modeling and remote sensing applications.

Data Availability Statement

Model input

Sea ice concentration data are available at DiGirolamo et al. (2022). Sea ice motion vectors are available at Tschudi et al. (2019). Atmospheric forcing data are available at Global Modeling And Assimilation Office (GMAO) (2015a, 2015b). Daily ocean heat flux data were downloaded from ECMWF.

Model output

Interannual variations of EASE-grid snow depth, snow density, and snow-ice thickness from 1 August 1980 through 31 July 2022 presented in this paper are available at Merkouriadi et al. (2023).

Altimetry input

CryoSat-2 Level 1B Baseline D/E SAR and SARIn data are available at European Space Agency (2019a, 2019b, 2019c, 2019d). Mean dynamic topography data are available at Knudsen et al. (2022). Sea ice concentration and type data are available at OSI SAF (2017a, 2017b), respectively. Python processing library pysiral is available at Hendricks et al. (2021).

Evaluation

Airborne data are available at Jutila et al. (2021a, 2021b); Jutila et al. (2021a, 2021b) for AWI IceBird and at Kurtz et al. (2015, 2016) for NASA OIB. SIMBA buoy data were obtained from `https://www.meereisportal.de` and Lei et al. (2021, 2022, 2023).

Acknowledgments

IM was supported by the ESA grant CCI+ 4000126449/19/I-NB. IM and AJ were supported by the Research Council of Finland grant 341550. GEL was supported by the United States National Science Foundation grant 1820927. AP was supported by the European Union's Horizon 2020 research and innovation programme under grant 101003472. The authors are grateful for Bin Cheng for providing the software code for the model HIGHTSI. Autonomous sea ice measurements (temperature profile and heating cycle data) from 2012 to 2020 were obtained from `https://www.meereisportal.de` (grant: REKLIM-2013-04). Scientific, colour-vision deficiency friendly, and perceptually-uniform color maps used in the figures of this manuscript were provided by Crameri (2023).

References

Blanchard-Wrigglesworth, E., Farrell, S. L., Newman, T., & Bitz, C. M. (2015). Snow cover on Arctic sea ice in observations and an Earth System Model. *Geophysical Research Letters*, *42*, 10,342–10,348. doi: 10.1002/2015GL066049

Blanchard-Wrigglesworth, E., Webster, M. A., Farrell, S. L., & Bitz, C. M. (2018). Reconstruction of Snow on Arctic Sea Ice. *Journal of Geophysical Research: Oceans*, *123*, 3588–3602. doi: 10.1002/2017JC013364

Briegleb, B., Bitz, C., Hunke, E., Lipscomb, W., Holland, M., Schramm, J., & Moritz, R. (2004). *Scientific Description of the Sea Ice Component in the Community Climate System Model, Version 3* (Tech. Rep.). University Corporation for Atmospheric Research. doi: 10.5065/D6HH6H1P

Cheng, B., Mäkynen, M., Similä, M., Rontu, L., & Vihma, T. (2013). Modelling snow and ice thickness in the coastal Kara Sea, Russian Arctic. *Annals of Glaciology*, *54*, 105–113. doi: 10.3189/2013AoG62A180

Cheng, B., Vihma, T., Zhanhai, Z., Zhijun, L., & Huiding, W. (2008). Snow and sea ice thermodynamics in the Arctic: Model validation and sensitivity study against SHEBA data. *Advances in Polar Science*, *19*, 108-122. Retrieved from `https://aps.chinare.org.cn/EN/Y2008/V19/I2/108`

Cheng, B., Zhang, Z., Vihma, T., Johansson, M., Bian, L., Li, Z., & Wu, H. (2008). Model experiments on snow and ice thermodynamics in the Arctic Ocean with CHINARE 2003 data. *Journal of Geophysical Research*, *113*, C09020. doi: 10.1029/2007JC004654

Clemens-Sewall, D., Polashenski, C., Frey, M. M., Cox, C. J., Granskog, M. A., Macfarlane, A. R., ... Perovich, D. (2023). Snow Loss Into Leads in Arctic Sea Ice: Minimal in Typical Wintertime Conditions, but High During a Warm and Windy Snowfall Event. *Geophysical Research Letters*, *50*, e2023GL102816. doi: 10.1029/2023GL102816

Crameri, F. (2023). *Scientific colour maps.* Zenodo. doi: 10.5281/ZENODO.1243862

DiGirolamo, N., Parkinson, C., Cavalieri, D., Gloersen, P., & Zwally, H. (2022). *Sea Ice Concentrations from Nimbus-7 SMMR and DMSP SSM/I-SSMIS Passive Microwave Data, Version 2* [data set]. NASA National Snow and Ice Data Center Distributed Active Archive Center. (Accessed: 2 April 2023) doi: 10.5067/MPYG15WAA4WX

European Space Agency. (2019a). *L1b SARin Precise Orbit. Baseline D.* [data set]. (Accessed: 29 October 2023) doi: 10.5270/cr2-u3805kw

European Space Agency. (2019b). *L1b SARin Precise Orbit. Baseline E.* [data set]. (Accessed: 29 October 2023) doi: 10.5270/CR2-6afef01

European Space Agency. (2019c). *L1b SAR Precise Orbit. Baseline D.* [data set]. (Accessed: 29 October 2023) doi: 10.5270/cr2-2cnblvi

European Space Agency. (2019d). *L1b SAR Precise Orbit. Baseline E.* [data set]. (Accessed: 29 October 2023) doi: 10.5270/CR2-fbae3cd

Gelaro, R., McCarty, W., Suárez, M. J., Todling, R., Molod, A., Takacs, L., ... Zhao, B. (2017). The Modern-Era Retrospective Analysis for Research and Applications, Version 2 (MERRA-2). *Journal of Climate*, *30*, 5419–5454. doi: 10.1175/JCLI-D-16-0758.1

Giles, K., Laxon, S., Wingham, D., Wallis, D., Krabill, W., Leuschen, C., ... Raney, R. (2007). Combined airborne laser and radar altimeter measurements over the Fram Strait in May 2002. *Remote Sensing of Environment*, *111*, 182–194. doi: 10.1016/j.rse.2007.02.037

Global Modeling And Assimilation Office (GMAO). (2015a). *MERRA-2 tavg1_2d_flx_Nx: 2d, 1-Hourly, Time-Averaged, Single-Level, Assimilation, Surface Flux Diagnostics V5.12.4* [data set]. NASA Goddard Earth Sciences Data and Information Services Center. (Accessed: 7 January 2023) doi: 10.5067/7MCPBJ41Y0K6

Global Modeling And Assimilation Office (GMAO). (2015b). *MERRA-2 tavg1_2d_slv_Nx: 2d, 1-Hourly, Time-Averaged, Single-Level, Assimilation, Single-Level Diagnostics V5.12.4* [data set]. NASA Goddard Earth Sciences Data and Information Services Center. (Accessed: 7 January 2023) doi: 10.5067/VJAFPLI1CSIV

Graham, R. M., Rinke, A., Cohen, L., Hudson, S. R., Walden, V. P., Granskog, M. A., ... Maturilli, M. (2017). A comparison of the two Arctic atmospheric winter states observed during N-ICE2015 and SHEBA. *Journal of Geophysical Research: Atmospheres*, *122*, 5716–5737. doi: 10.1002/2016JD025475

Granskog, M. A., Rösel, A., Dodd, P. A., Divine, D., Gerland, S., Martma, T., & Leng, M. J. (2017). Snow contribution to first-year and second-year Arctic sea ice mass balance north of Svalbard. *Journal of Geophysical Research: Oceans*, *122*, 2539–2549. doi: 10.1002/2016JC012398

Grenfell, T. C., & Maykut, G. A. (1977). The Optical Properties of Ice and Snow in the Arctic Basin. *Journal of Glaciology*, *18*, 445–463. doi: 10.3189/S0022143000021122

Grosfeld, K., Treffeisen, R., Asseng, J., Bartsch, A., Bräuer, B., Fritzsch, B., ... Weigelt, M. (2016). Online Sea-Ice Knowledge and Data Platform. *Polarforschung; 85*. doi: 10.2312/POLFOR.2016.011

Hendricks, S., Sallila, H., Brockley, D., & Paul, S. (2021). *shendric/pysiral: Product update (C3S, AWI, CCI, CryoTEMPO)* [software]. Zenodo. (Accessed: 29 October 2023) doi: 10.5281/zenodo.5566347

Hersbach, H., Bell, B., Berrisford, P., Hirahara, S., Horányi, A., Muñoz-Sabater, J.,

… Thépaut, J. (2020). The ERA5 global reanalysis. *Quarterly Journal of the Royal Meteorological Society*, *146*, 1999–2049. doi: 10.1002/qj.3803

Itkin, P., Spreen, G., Cheng, B., Doble, M., Girard-Ardhuin, F., Haapala, J., … Wilkinson, J. (2017). Thin ice and storms: Sea ice deformation from buoy arrays deployed during N-ICE2015. *Journal of Geophysical Research: Oceans*, *122*, 4661–4674. doi: 10.1002/2016JC012403

Jackson, K., Wilkinson, J., Maksym, T., Meldrum, D., Beckers, J., Haas, C., & Mackenzie, D. (2013). A novel and low-cost sea ice mass balance buoy. *Journal of Atmospheric and Oceanic Technology*, *30*, 2676-2688. doi: 10.1175/JTECH-D-13-00058.1

Jutila, A., Hendricks, S., Ricker, R., von Albedyll, L., & Haas, C. (2021a). *Airborne sea ice parameters during the IceBird Winter 2019 campaign in the Arctic Ocean, version 1* [data set]. PANGAEA. (Accessed: 18 July 2023) doi: 10.1594/PANGAEA.933912

Jutila, A., Hendricks, S., Ricker, R., von Albedyll, L., & Haas, C. (2021b). *Airborne sea ice parameters during the PAMARCMIP2017 campaign in the Arctic Ocean, version 1* [data set]. PANGAEA. (Accessed: 18 July 2023) doi: 10.1594/PANGAEA.933883

Jutila, A., Hendricks, S., Ricker, R., von Albedyll, L., Krumpen, T., & Haas, C. (2022). Retrieval and parameterisation of sea-ice bulk density from airborne multi-sensor measurements. *The Cryosphere*, *16*, 259-275. doi: 10.5194/tc-16-259-2022

Jutila, A., King, J., Paden, J., Ricker, R., Hendricks, S., Polashenski, C., … Haas, C. (2022). High-Resolution Snow Depth on Arctic Sea Ice From Low-Altitude Airborne Microwave Radar Data. *IEEE Transactions on Geoscience and Remote Sensing*, *60*, 1-16. doi: 10.1109/TGRS.2021.3063756

Jutila, A., King, J., Ricker, R., Hendricks, S., Helm, V., Binder, T., & Haas, C. (2021a). *Airborne snow depth on sea ice during the IceBird Winter 2019 campaign in the Arctic Ocean, Version 1.* PANGAEA. (Accessed: 18 July 2023) doi: 10.1594/PANGAEA.932790

Jutila, A., King, J., Ricker, R., Hendricks, S., Helm, V., Binder, T., & Herber, A. (2021b). *Airborne snow depth on sea ice during the PAMARCMIP2017 campaign in the Arctic Ocean, Version 1.* PANGAEA. (Accessed: 18 July 2023) doi: 10.1594/PANGAEA.932668

Knudsen, P., Andersen, O., Maximenko, N., & Hafne, J. (2022). *A new combined mean dynamic topography model — DTUUH22MDT* [data set]. Retrieved from `https://ftp.spacecenter.dk/pub/DTU22/MDT/` (Accessed: 29 October 2023)

Kurtz, N. T., Markus, T., Cavalieri, D. J., Sparling, L. C., Krabill, W. B., Gasiewski, A. J., & Sonntag, J. G. (2009). Estimation of sea ice thickness distributions through the combination of snow depth and satellite laser altimetry data. *Journal of Geophysical Research*, *114*, C10007. doi: 10.1029/2009JC005292

Kurtz, N. T., Studinger, M., Harbeck, J., DePaul Onana, V., & Yi, D. (2015). *IceBridge L4 Sea Ice Freeboard, Snow Depth, and Thickness, Version 1.* NASA National Snow and Ice Data Center Distributed Active Archive Center. (Accessed: 18 July 2023) doi: 10.5067/G519SHCKWQV6

Kurtz, N. T., Studinger, M., Harbeck, J., DePaul Onana, V., & Yi, D. (2016). *IceBridge Sea Ice Freeboard, Snow Depth, and Thickness Quick Look, Version 1.* NASA National Snow and Ice Data Center Distributed Active Archive Center. Retrieved from `https://nsidc.org/data/NSIDC-0708/versions/1` (Accessed: 18 July 2023) doi: 10.5067/GRIXZ91DE0L9

Kwok, R., & Cunningham, G. F. (2008). ICESat over Arctic sea ice: Estimation of snow depth and ice thickness. *Journal of Geophysical Research*, *113*, C08010. doi: 10.1029/2008JC004753

Kwok, R., Cunningham, G. F., Wensnahan, M., Rigor, I., Zwally, H. J., & Yi, D. (2009). Thinning and volume loss of the Arctic Ocean sea ice cover: 2003–2008. *Journal of Geophysical Research*, *114*, C07005. doi: 10.1029/2009JC005312

Kwok, R., Spreen, G., & Pang, S. (2013). Arctic sea ice circulation and drift speed: Decadal trends and ocean currents. *Journal of Geophysical Research: Oceans*, *118*, 2408–2425. doi: 10.1002/jgrc.20191

Landy, J. C., Dawson, G. J., Tsamados, M., Bushuk, M., Stroeve, J. C., Howell, S. E. L., … Aksenov, Y. (2022). A year-round satellite sea-ice thickness record from CryoSat-2. *Nature*, *609*(7927), 517–522. doi: 10.1038/s41586-022-05058-5

Landy, J. C., Petty, A. A., Tsamados, M., & Stroeve, J. C. (2020). Sea Ice Roughness Overlooked as a Key Source of Uncertainty in CryoSat-2 Ice Freeboard Retrievals. *Journal of Geophysical Research: Oceans*, *125*, e2019JC015820. doi: 10.1029/2019JC015820

Launiainen, J., & Cheng, B. (1998). Modelling of ice thermodynamics in natural water bodies. *Cold Regions Science and Technology*, *27*, 153–178. doi: 10.1016/S0165-232X(98)00009-3

Laxon, S., Peacock, N., & Smith, D. (2003). High interannual variability of sea ice thickness in the Arctic region. *Nature*, *425*, 947–950. doi: 10.1038/nature02050

Lei, R., Cheng, B., Hoppmann, M., Nicolaus, M., & Regnery, J. (2023). *Temperature and heating induced temperature difference measurements from SIMBA-type sea ice mass balance buoy 2020T84, deployed during MOSAiC 2020/21* [data set]. PANGAEA. (Accessed: 6 September 2023) doi: 10.1594/PANGAEA.958397

Lei, R., Cheng, B., Hoppmann, M., & Zuo, G. (2021). *Temperature and heating induced temperature difference measurements from SIMBA-type sea ice mass balance buoy 2019T69, deployed during MOSAiC 2019/20* [data set]. PANGAEA. (Accessed: 6 September 2023) doi: 10.1594/PANGAEA.938096

Lei, R., Cheng, B., Hoppmann, M., & Zuo, G. (2022). *Temperature and heating induced temperature difference measurements from SIMBA-type sea ice mass balance buoy 2019T72, deployed during MOSAiC 2019/20* [data set]. PANGAEA. (Accessed: 6 September 2023) doi: 10.1594/PANGAEA.940668

Leppäranta, M. (1983). A Growth Model for Black Ice, Snow Ice and Snow Thickness in Subarctic Basins. *Hydrology Research*, *14*, 59–70. doi: 10.2166/nh.1983.0006

Liston, G. E., & Elder, K. (2006a). A Distributed Snow-Evolution Modeling System (SnowModel). *Journal of Hydrometeorology*, *7*, 1259–1276. doi: 10.1175/JHM548.1

Liston, G. E., & Elder, K. (2006b). A Meteorological Distribution System for High-Resolution Terrestrial Modeling (MicroMet). *Journal of Hydrometeorology*, *7*(2), 217–234. doi: 10.1175/JHM486.1

Liston, G. E., Itkin, P., Stroeve, J., Tschudi, M., Stewart, J. S., Pedersen, S. H., … Elder, K. (2020). A Lagrangian Snow-Evolution System for Sea-Ice Applications (SnowModel-LG): Part I — Model Description. *Journal of Geophysical Research: Oceans*, *125*, e2019JC015913. doi: 10.1029/2019JC015913

Liston, G. E., Polashenski, C., Rösel, A., Itkin, P., King, J., Merkouriadi, I., & Haapala, J. (2018). A Distributed Snow-Evolution Model for Sea-Ice Applications (SnowModel). *Journal of Geophysical Research: Oceans*, *123*, 3786–3810. doi: 10.1002/2017JC013706

Liston, G. E., Stroeve, J., & Itkin, P. (2020). *Lagrangian Snow Distributions for Sea-Ice Applications* [data set]. NASA National Snow and Ice Data Center Distributed Active Archive Center. doi: 10.5067/27A0P5M6LZBI

Macfarlane, A. R., Schneebeli, M., Dadic, R., Tavri, A., Immerz, A., Polashenski, C., … Fons, S. (2023). A Database of Snow on Sea Ice in the Central Arctic Collected during the MOSAiC expedition. *Scientific Data*, *10*, 398. doi: 10.1038/s41597-023-02273-1

MacGregor, J. A., Boisvert, L. N., Medley, B., Petty, A. A., Harbeck, J. P., Bell, R. E., … Yungel, J. K. (2021). The Scientific Legacy of NASA's Operation IceBridge. *Reviews of Geophysics*, *59*. doi: 10.1029/2020RG000712

Markus, T., Neumann, T., Martino, A., Abdalati, W., Brunt, K., Csatho, B., … Zwally, J. (2017). The Ice, Cloud, and land Elevation Satellite-2 (ICESat-2): Science requirements, concept, and implementation. *Remote Sensing of Environment*, *190*, 260–273. doi: 10.1016/j.rse.2016.12.029

Maslanik, J. A., Fowler, C., Stroeve, J., Drobot, S., Zwally, J., Yi, D., & Emery, W. (2007). A younger, thinner Arctic ice cover: Increased potential for rapid, extensive sea-ice loss. *Geophysical Research Letters*, *34*, L24501. doi: 10.1029/2007GL032043

Maykut, G. A., & Untersteiner, N. (1971). Some results from a time-dependent thermodynamic model of sea ice. *Journal of Geophysical Research*, *76*, 1550–1575. doi: 10.1029/JC076i006p01550

Meier, W. N., Hovelsrud, G. K., van Oort, B. E., Key, J. R., Kovacs, K. M., Michel, C., … Reist, J. D. (2014). Arctic sea ice in transformation: A review of recent observed changes and impacts on biology and human activity. *Reviews of Geophysics*, *52*, 185–217. doi: 10.1002/2013RG000431

Merkouriadi, I., Cheng, B., Graham, R. M., Rösel, A., & Granskog, M. A. (2017). Critical Role of Snow on Sea Ice Growth in the Atlantic Sector of the Arctic Ocean. *Geophysical Research Letters*, *44*, 10,479–10,485. doi: 10.1002/2017GL075494

Merkouriadi, I., Liston, G. E., Graham, R. M., & Granskog, M. A. (2020). Quantifying the Potential for Snow-Ice Formation in the Arctic Ocean. *Geophysical Research Letters*, *47*, e2019GL085020. doi: 10.1029/2019GL085020

Merkouriadi, I., Liston, G. E., & Jutila, A. (2023). *Investigating the effect of snow-ice formation on snow depth and density over Arctic sea ice* [data set]. Finnish Meteorological Institute. doi: 10.57707/fmi-b2share.529adcd77c144d82a7b29841e34922a3

OSI SAF. (2017a). *Global Sea Ice Concentration (netCDF) - DMSP* [data set]. OSI SAF. (Accessed: 29 October 2023) doi: 10.15770/EUM_SAF_OSI_NRT_2004

OSI SAF. (2017b). *Global Sea Ice Type (netCDF) - Multimission* [data set]. OSI SAF. (Accessed: 29 October 2023) doi: 10.15770/EUM_SAF_OSI_NRT_2006

Perovich, D. K. (1996). *The optical properties of sea ice* (Tech. Rep.). Cold Regions Research and Engineering Laboratory. Retrieved from `http://hdl.handle.net/11681/2648`

Petty, A. A., Webster, M., Boisvert, L., & Markus, T. (2018). The NASA Eulerian Snow on Sea Ice Model (NESOSIM) v1.0: initial model development and analysis. *Geoscientific Model Development*, *11*, 4577–4602. doi: 10.5194/gmd-11-4577-2018

Pringle, D. J., Eicken, H., Trodahl, H. J., & Backstrom, L. G. E. (2007). Thermal conductivity of landfast Antarctic and Arctic sea ice. *Journal of Geophysical Research*, *112*, C04017. doi: 10.1029/2006JC003641

Provost, C., Sennéchael, N., Miguet, J., Itkin, P., Rösel, A., Koenig, Z., … Granskog, M. A. (2017). Observations of flooding and snow-ice formation in a thinner Arctic sea-ice regime during the N-ICE 2015 campaign: Influence of basal ice melt and storms. *Journal of Geophysical Research: Oceans*, *122*, 7115–7134. doi: 10.1002/2016JC012011

Rampal, P., Weiss, J., & Marsan, D. (2009). Positive trend in the mean speed and deformation rate of Arctic sea ice, 1979–2007. *Journal of Geophysical Research*, *114*, C05013. doi: 10.1029/2008JC005066

Rinke, A., Maturilli, M., Graham, R. M., Matthes, H., Handorf, D., Cohen, L.,

… Moore, J. C. (2017). Extreme cyclone events in the Arctic: Wintertime variability and trends. *Environmental Research Letters*, *12*, 094006. doi: 10.1088/1748-9326/aa7def

Saloranta, T. M. (2000). Modeling the evolution of snow, snow ice and ice in the Baltic Sea. *Tellus A: Dynamic Meteorology and Oceanography*, *52*, 93. doi: 10.3402/tellusa.v52i1.12255

Stroeve, J. C., Liston, G. E., Buzzard, S., Zhou, L., Mallett, R., Barrett, A., … Stewart, J. S. (2020). A Lagrangian Snow Evolution System for Sea Ice Applications (SnowModel-LG): Part II — Analyses. *Journal of Geophysical Research: Oceans*, *125*, e2019JC015900. doi: 10.1029/2019JC015900

Stroeve, J. C., Markus, T., Boisvert, L., Miller, J., & Barrett, A. (2014). Changes in Arctic melt season and implications for sea ice loss. *Geophysical Research Letters*, *41*, 1216–1225. doi: 10.1002/2013GL058951

Tschudi, M., Meier, W. N., & Stewart, J. S. (2020). An enhancement to sea ice motion and age products at the National Snow and Ice Data Center (NSIDC). *The Cryosphere*, *14*(5), 1519–1536. doi: 10.5194/tc-14-1519-2020

Tschudi, M., Meier, W. N., Stewart, J. S., Fowler, C., & Maslanik, J. (2019). *Polar Pathfinder Daily 25 km EASE-Grid Sea Ice Motion Vectors, Version 4* [data set]. NASA National Snow and Ice Data Center Distributed Active Archive Center. (Accessed: 20 March 2023) doi: 10.5067/INAWUWO7QH7B

Wang, C., Cheng, B., Wang, K., Gerland, S., & Pavlova, O. (2015). Modelling snow ice and superimposed ice on landfast sea ice in Kongsfjorden, Svalbard. *Polar Research*, *34*, 20828. doi: 10.3402/polar.v34.20828

Warren, S. G., Rigor, I. G., Untersteiner, N., Radionov, V. F., Bryazgin, N. N., Aleksandrov, Y. I., & Colony, R. (1999). Snow Depth on Arctic Sea Ice. *Journal of Climate*, *12*, 1814–1829. doi: 10.1175/1520-0442(1999)012⟨1814:SDOASI⟩2.0.CO;2

Webster, M. A., Parker, C., Boisvert, L., & Kwok, R. (2019). The role of cyclone activity in snow accumulation on Arctic sea ice. *Nature Communications*, *10*, 5285. doi: 10.1038/s41467-019-13299-8

Webster, M. A., Rigor, I. G., Nghiem, S. V., Kurtz, N. T., Farrell, S. L., Perovich, D. K., & Sturm, M. (2014). Interdecadal changes in snow depth on Arctic sea ice. *Journal of Geophysical Research: Oceans*, *119*, 5395–5406. doi: 10.1002/2014JC009985

Willatt, R., Giles, K., Laxon, S., Stone-Drake, L., & Worby, A. (2010). Field Investigations of Ku-Band Radar Penetration Into Snow Cover on Antarctic Sea Ice. *IEEE Transactions on Geoscience and Remote Sensing*, *48*, 365–372. doi: 10.1109/TGRS.2009.2028237

Woods, C., & Caballero, R. (2016). The Role of Moist Intrusions in Winter Arctic Warming and Sea Ice Decline. *Journal of Climate*, *29*, 4473–4485. doi: 10.1175/JCLI-D-15-0773.1

Zuo, H., Balmaseda, M. A., Tietsche, S., Mogensen, K., & Mayer, M. (2019). The ECMWF operational ensemble reanalysis–analysis system for ocean and sea ice: a description of the system and assessment. *Ocean Science*, *15*(3), 779–808. doi: 10.5194/os-15-779-2019

Zygmuntowska, M., Rampal, P., Ivanova, N., & Smedsrud, L. H. (2014). Uncertainties in Arctic sea ice thickness and volume: new estimates and implications for trends. *The Cryosphere*, *8*, 705–720. doi: 10.5194/tc-8-705-2014

Figure_1.

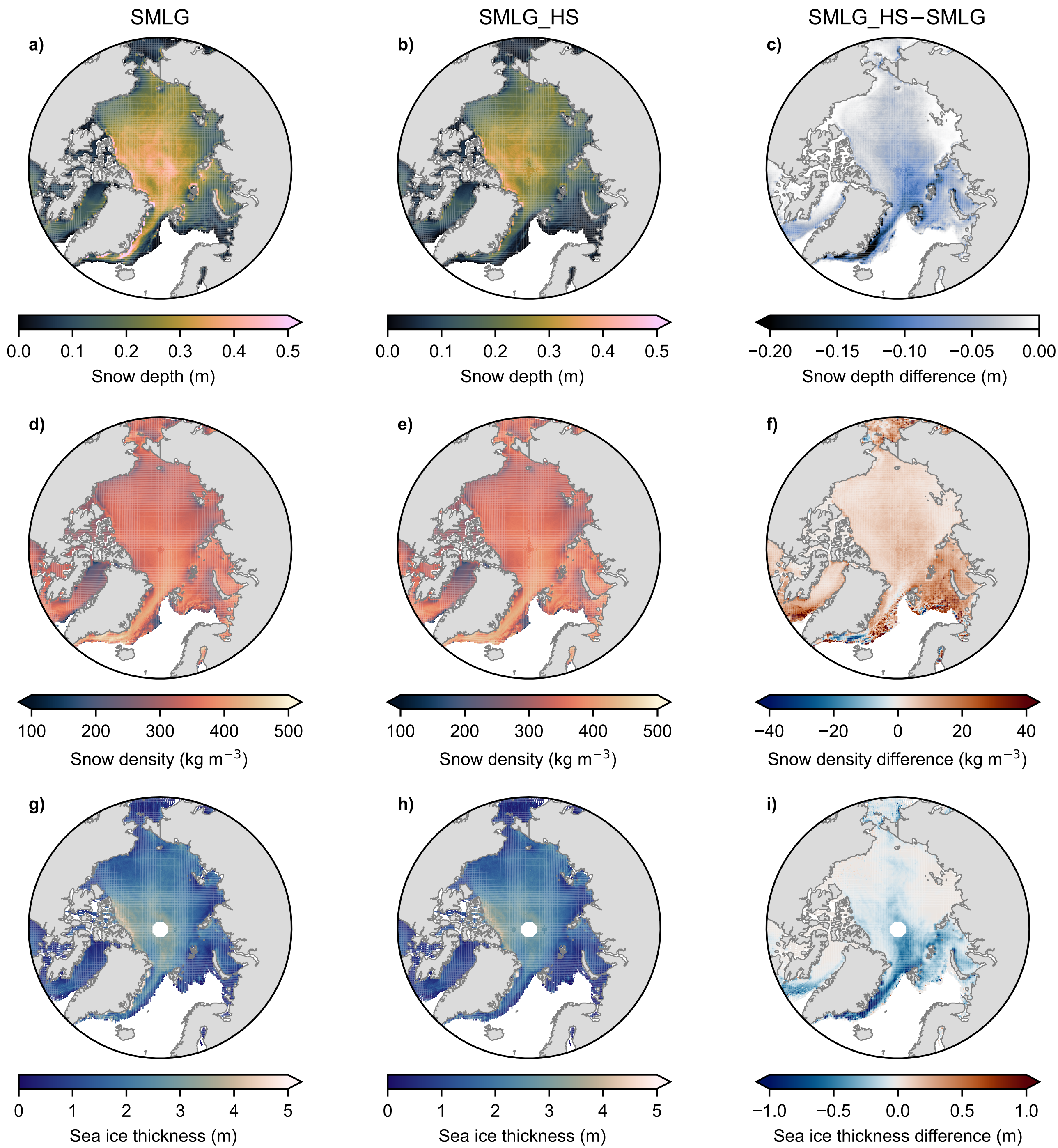

SMLG
SMLG_HS
SMLG_HS−SMLG
a)
b)
c)
0.0 0.1 0.2 0.3 0.4 0.5
Snow depth (m)
0.0 0.1 0.2 0.3 0.4 0.5
Snow depth (m)
−0.20 −0.15 −0.10 −0.05 0.00
Snow depth difference (m)
d)
e)
f)
100 200 300 400 500
Snow density (kg m^{-3})
100 200 300 400 500
Snow density (kg m^{-3})
−40 −20 0 20 40
Snow density difference (kg m^{-3})
g)
h)
i)
0 1 2 3 4 5
Sea ice thickness (m)
0 1 2 3 4 5
Sea ice thickness (m)
−1.0 −0.5 0.0 0.5 1.0
Sea ice thickness difference (m)

Figure_2.

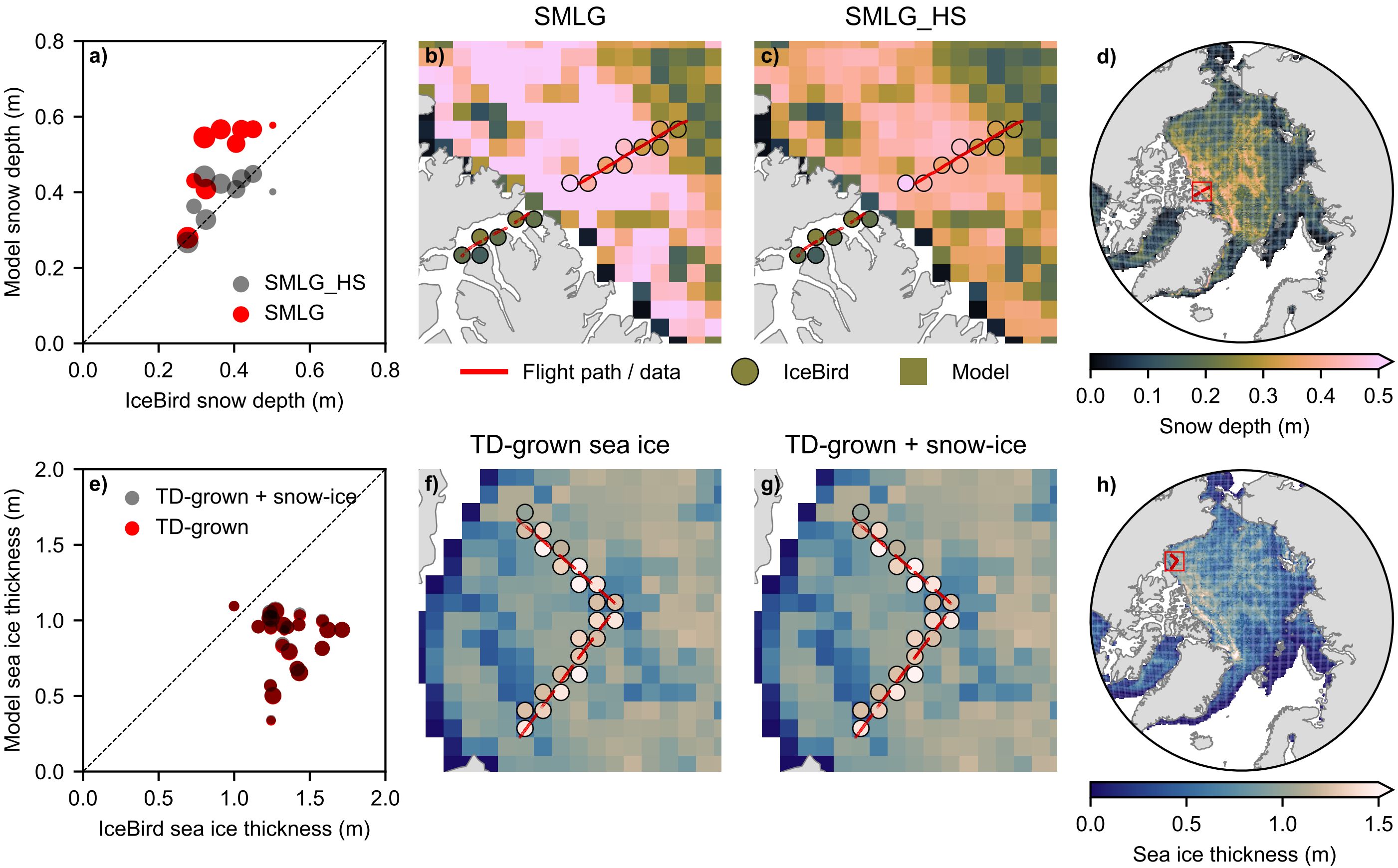

SMLG
SMLG_HS
a)
b)
c)
d)
Model snow depth (m)
IceBird snow depth (m)
SMLG_HS
SMLG
Flight path / data
IceBird
Model
Snow depth (m)
TD-grown sea ice
TD-grown + snow-ice
e)
f)
g)
h)
TD-grown + snow-ice
TD-grown
Model sea ice thickness (m)
IceBird sea ice thickness (m)
Sea ice thickness (m)

Investigating the Effect of Snow-Ice Formation on Snow Depth and Density over Arctic Sea Ice

I. Merkouriadi[1], G. E. Liston[2], A. Jutila[1], H. Sallila[1], A. Preußer[3]

[1]Finnish Meteorological Institute, Helsinki, Finland
[2]Cooperative Institute for Research in the Atmosphere, Colorado State University, Fort Collins, CO, USA
[3]Alfred-Wegener-Institut, Helmholtz-Zentrum für Polar- und Meeresforschung, Bremerhaven, Germany

Key Points:

- We examined the changes in modeled snow depth and density over sea ice caused by snow-ice formation.
- Accounting for snow and sea ice interactions markedly reduces snow depth on level ice.
- Sea ice thickness retrievals from radar altimetry change on average by 7.7 % when snow products account for snow-ice.

Corresponding author: Ioanna Merkouriadi, `ioanna.merkouriadi@fmi.fi`

Abstract

We examined the effect of snow-ice formation on SnowModel-LG snow depth and density products. We coupled SnowModel-LG, a modeling system adapted for snow depth and density reconstruction over sea ice, with HIGHTSI, a 1-D thermodynamic sea ice model, to create SnowModel-LG_HS. Pan-Arctic model simulations spanned from 1 August 1980 through 31 July 2022. In SnowModel-LG_HS, domain average snow depth decreased by 20 %, and snow density increased by 2 % when compared to SnowModel-LG, with largest differences in the Atlantic sector. Averaged across the CryoSat-2 era (2011–2022), domain average April sea ice thickness retrievals from CryoSat-2 decreased by 7.7 % when snow-ice was accounted for. Evaluation of SnowModel-LG_HS against snow depth, snow-ice, and sea ice thickness observations highlighted the importance of snow redistribution over deformed sea ice. The findings suggest that neglecting snow and sea ice interactions in models can lead to substantial overestimation of snow depth over level ice.

Plain Language Summary

The amount of snow on sea ice is important for monitoring sea ice thickness, which is one of the key factors in a changing climate. Recent advances in snow-on-sea-ice modeling have made it possible to simulate snow depth and density over Arctic sea ice. However, these simulations often do not consider how much snow is lost to snow and sea ice interactions, such as snow-ice formation. Snow-ice forms when snow becomes part of the sea ice, after seawater floods the sea ice surface and freezes inside the snow. In this study, we combined a snow model with a sea ice model to understand how snow changes when snow-ice forms. Our results show that when snow-ice forms, snow depth decreases, and snow density commonly increases. The differences are highest in the Atlantic sector of the Arctic, where snow-ice is more likely to form due to high annual snowfall.

1 Introduction

Arctic sea ice is going through unprecedented changes, decreasing dramatically both in extent (e.g. Stroeve et al., 2014) and in thickness (Kwok et al., 2009; Maslanik et al., 2007), and transitioning from a multiyear ice to a seasonal, first-year ice system (Meier et al., 2014). The role of snow cover over thinner, seasonal sea ice is amplified in many ways. First, the thermal resistance of snow cover becomes a dominant control over the atmosphere-ocean heat fluxes, regulating sea ice growth in winter. Second, the snow load becomes more likely to submerge thinner ice underneath the water level, creating negative freeboard conditions. If sea water floods at the ice/snow interface and freezes there, snow-ice is formed, that is a mixture of frozen seawater and snow (e.g. Leppäranta, 1983). Snow-ice is a common phenomenon in seas that are seasonally covered by ice (i.e., Baltic Sea, Sea of Okhotsk), but it was not commonly observed in drifting Arctic sea ice until the Norwegian Young Sea ICE (N-ICE2015) expedition (Granskog et al., 2017; Provost et al., 2017). Snow-ice is a sink for snow, and it can contribute significantly to the sea ice mass balance (Merkouriadi et al., 2017, 2020). Therefore, it is essential to consider it for improving Arctic sea ice forecasts.

Satellite altimetry is the most common method for monitoring sea ice thickness, providing nearly full coverage of the Arctic Ocean (Landy et al., 2022; Laxon et al., 2003; Markus et al., 2017). Information on the snow load exerted on sea ice is crucial for altimetry retrievals of sea ice thickness, because radar and laser altimeters, in principle, measure ice or snow freeboard; the elevation of the ice or snow surface from the water surface. Snow depth and density are required to convert freeboard to sea ice thickness information (e.g. Kurtz et al., 2009). According to Giles et al. (2007), uncertainties in snow depth and density contribute 48 % and 14 %, respectively, to the total error of sea ice thickness retrievals from radar altimetry. A more recent study by Landy et al. (2020)

estimated these uncertainties at 11 % for snow depth and 16 % for density. Similarly, snow depth and density uncertainties were found to contribute 70 % and 30–35 %, respectively, to the total error of sea ice thickness retrievals from laser altimetry (Zygmuntowska et al., 2014).

Snow depth and density estimates used in altimetry applications are often derived from snow climatologies or their modified versions. The most widely used snow-on-sea-ice climatology is compiled from a snow depth and density data set collected decades ago mostly over multiyear ice (Warren et al., 1999). In a changing Arctic sea ice system, snow conditions are expected to change as well (Blanchard-Wrigglesworth et al., 2015; Webster et al., 2014), and these changes are not captured by the Warren et al. (1999) climatology. In addition to the long-term changes, climatology overlooks the spatio-temporal differences and interannual variability of snow conditions in the Arctic, which are evidently strong (Webster et al., 2019). Addressing the imperative need for better representation of snow on sea ice, efforts have focused on reanalysis-based snow depth and density reconstructions (e.g. Blanchard-Wrigglesworth et al., 2018; Kwok & Cunningham, 2008; Petty et al., 2018). A recent contribution was SnowModel-LG, a state-of-the-art Lagrangian snow evolution model (Liston, Itkin, et al., 2020). Compared to other reanalysis-based products, SnowModel-LG implemented higher resolution Lagrangian parcel tracking and included an improved representation of snow evolution physics. It has been bias-corrected and validated against a wide observation framework, and yielded good agreement, especially with in situ measurements (Stroeve et al., 2020). However, neither SnowModel-LG nor any of the above-mentioned snow products account for snow losses due to snow and sea ice interactions, such as snow-ice formation.

This study aims to examine snow loss through snow-ice formation, and its effect in SnowModel-LG snow depth and density simulations over the Arctic Ocean, from 1 August 1980 through 31 July 2022. To investigate this, we coupled SnowModel-LG with the High-Resolution Thermodynamic Sea Ice model (HIGHTSI) (Launiainen & Cheng, 1998) to produce SnowModel-LG_HS. In HIGHTSI, snow-ice forms when the sea ice surface is depressed below the water surface (negative freeboard), with the assumption that all negative freeboard will result in flooding and, consequently, snow-ice formation. We investigated the effect of both snow depth and density products (SnowModel-LG and SnowModel-LG_HS) on sea ice thickness retrievals from satellite radar altimetry (CryoSat-2). We discuss the results in light of an evaluation exercise we performed using observations from airborne campaigns and drifting ice mass balance buoys (IMBs).

2 Materials and Methods

2.1 SnowModel-LG

SnowModel is a collection of snow distribution and snow evolution modeling tools, applicable to any environment experiencing snow, including sea ice applications (Liston & Elder, 2006a). SnowModel-LG is adapted for snow depth and density reconstruction over sea ice (Liston, Itkin, et al., 2020). It is implemented in a Lagrangian framework to simulate snow properties on drifting sea ice. SnowModel-LG accounts for physical snow processes such as sublimation from static surfaces and blowing snow, snow melt, evolution of snow density and temperature profiles, energy and mass transfers within the snowpack, and superimposed ice formation in a multi-layer configuration.

At each time step (3-hour here), SnowModel-LG performs a mass-budget calculation, where snow water equivalent (SWE) depth (m) is defined by snow mass gains, losses, and ice parcel dynamics,

$$\frac{\mathrm{d}SWE}{\mathrm{d}t} = \frac{1}{\rho_w}\left[(P_r + P_s) - (S_{ss} + S_{bs} + M) + D\right] \tag{1}$$

where t (s) is time; $\rho_w = 1{,}000\,\mathrm{kg\,m^{-3}}$ is the water density; P_r ($\mathrm{kg\,m^{-2}\,s^{-1}}$) and P_s ($\mathrm{kg\,m^{-2}\,s^{-1}}$) are the water-equivalent rainfall and snowfall fluxes, respectively; S_{ss} ($\mathrm{kg\,m^{-2}\,s^{-1}}$) and S_{bs} ($\mathrm{kg\,m^{-2}\,s^{-1}}$) are the water-equivalent sublimation from static-surface and blowing-snow processes, respectively; M ($\mathrm{kg\,m^{-2}\,s^{-1}}$) is melt-related mass losses; and D ($\mathrm{kg\,m^{-2}\,s^{-1}}$) is mass losses and gains from sea ice dynamics processes (i.e., parcels being created and lost with ice motion, divergence, and convergence).

Snow depth h_s (m) is related to SWE through the ratio of snow (ρ_s), and water (ρ_w) densities,

$$SWE = \frac{\rho_s}{\rho_w} h_s. \tag{2}$$

Therefore, the evolution of snow depths and densities are calculated by

$$\frac{\mathrm{d}\left(\rho_s h_s\right)}{\mathrm{d}t} = \left(P_r + P_s\right) - \left(S_{ss} + S_{bs} + M\right) + D. \tag{3}$$

In SnowModel-LG, snow density evolves and changes in response to compaction (weight of the above snow layers), wind force, freezing of liquid water, and vapor flux through the snowpack. Additional information on the components and the configuration of SnowModel-LG are provided in detail in Liston, Itkin, et al. (2020). The model configuration in this study is identical to the one used in Liston, Itkin, et al. (2020), only here we have extended the simulation for another four years. According to Stroeve et al. (2020), SnowModel-LG performed well in capturing the spatial and seasonal variation of snow distributions, when evaluated against several Arctic data sets.

In the simulations presented herein, Lagrangian parcel tracking began on 1 August 1980. The first simulation year assumes no snow atop the sea ice; the following years carry available snow from 31 July to 1 August. Essential inputs are atmospheric reanalysis estimates of near-surface air temperature, relative humidity, precipitation, wind speed and direction, and sea ice motion and concentration products.

2.2 HIGHTSI

HIGHTSI is a 1-D thermodynamic sea ice model designed to simulate the evolution of snow and sea ice thickness and temperature profiles (Launiainen & Cheng, 1998) by solving the heat conduction equation for multiple ice and snow layers. The sea ice thermal conductivity is parameterized following Pringle et al. (2007). HIGHTSI simulates snow-ice formation following Saloranta (2000).

HIGHTSI has been widely used in process studies and validated extensively against observations (Cheng, Zhang, et al., 2008; Cheng et al., 2013; Merkouriadi et al., 2017, 2020; Wang et al., 2015). In this study, we used a model configuration that is derived from validation studies on Arctic sea ice. The model's vertical resolution has been found to be critical for its performance in the Arctic (Cheng, Vihma, et al., 2008). Here, we used 20 layers in the ice which is considered optimal for capturing internal thermodynamic processes (Cheng, Vihma, et al., 2008; Cheng, Zhang, et al., 2008; Cheng et al., 2013; Wang et al., 2015). Detailed information on model parameterizations is given in Table S1 in the supporting information (Briegleb et al., 2004; Cheng, Vihma, et al., 2008; Granskog et al., 2017; Grenfell & Maykut, 1977; Liston, Itkin, et al., 2020; Maykut & Untersteiner, 1971; Perovich, 1996; Pringle et al., 2007; Wang et al., 2015; Zuo et al., 2019).

Merkouriadi et al. (2020) implemented HIGHTSI in a Lagrangian framework to examine pan-Arctic snow-ice distributions. In the study presented herein, HIGHTSI was modified further, so that snow depth and density evolution were simulated by SnowModel-LG in a 25-layer configuration.

2.3 SnowModel-LG_HS

We performed two separate snow-on-sea-ice simulations. First, we simulated snow depth and density with SnowModel-LG (i.e. Liston, Itkin, et al., 2020). Second, SnowModel-LG's snow depth and density evolution were coupled with HIGHTSI's snow-ice and thermodynamic ice growth representations. The coupled modeling products are hereafter referred to as being created by SnowModel-LG_HS.

For the SnowModel-LG_HS runs, snow density was simulated following Appendix C of Liston, Itkin, et al. (2020), with the vertical density profile parameterized as being a linear fit between densities that are 20 % greater than the mean at the top of the snowpack (assumed to be wind slab), and 20 % less at the bottom of the snowpack (assumed to be depth hoar). These percentages are consistent with snow-pit measurements made during the Multidisciplinary drifting Observatory for the Study of Arctic Climate (MOSAiC) expedition (Macfarlane et al., 2023). This approach was chosen to provide a best-possible fit to available snow density observations, as opposed to relying completely on SnowModel-LG's representation of the vertical density evolution. To account for changes in snow density in response to snow-ice formation, when snow-ice was formed, the corresponding snow-depth amount was removed from the bottom layers of the snowpack, and the bulk density was recalculated based on the depth and density of the remaining snow. Additional model specifications are presented in the supporting information (Table S1).

2.4 Input Data Sets

Daily ice concentrations (15–100 %) by DiGirolamo et al. (2022) were used to define whether an ice parcel existed and whether snow could accumulate on that parcel. Ice motion vectors from the National Snow and Ice Data Center (NSIDC) (Tschudi et al., 2019, 2020) gridded over 25-km spatial resolution were used as Lagrangian ice parcel tracks. NASA's Modern Era Retrospective Analysis for Research and Application Version 2 (MERRA-2; Gelaro et al., 2017; Global Modeling And Assimilation Office (GMAO), 2015a, 2015b) was used as atmospheric forcing to SnowModel-LG_HS. Specifically, SnowModel-LG_HS was forced with 10-m wind speed and direction, 2-m air temperature and relative humidity, and total water-equivalent precipitation from MERRA-2. During these simulations, MicroMet (Liston & Elder, 2006b) provided the required liquid and solid precipitation, and the downwelling shortwave and longwave radiation following Liston, Itkin, et al. (2020).

We applied the same bias-correction in MERRA-2 reanalysis as in Liston, Itkin, et al. (2020), where observations from NASA Operation IceBridge (OIB; 2009–2016) were used to scale the precipitation inputs. In Liston, Itkin, et al. (2020), 8-year averages of precipitation scaling factors were calculated and they were applied over all ice parcels and through the whole simulation period, making the results of MERRA-2 and the European Centre for Medium-Range Weather Forecasts (ECMWF) ReAnalysis-5th Generation (ERA5; Hersbach et al., 2020) model runs similar. Scaling factors were 1.37 for MERRA-2 and 1.58 for ERA5, indicating the need to increase the precipitation inputs in order to match the OIB observations. The same scaling factors were used in this study for the results to be comparable with the publicly available SnowModel-LG snow depth and density data set (Liston, Stroeve, & Itkin, 2020).

For the ocean boundary forcing, at the ice/ocean interface, we used ocean heat flux from the Ocean Reanalysis System 5 (ORAS5) provided at the ECMWF (Zuo et al., 2019). ORAS5 resolution is eddy-permitting (0.25° latitude and longitude) horizontally and 1 m vertically. ORAS5 includes five ensemble members and covers the period from 1979 onward. In our study, we used the ensemble mean, providing one unique value on a 1° grid for each simulation day.

2.5 Model Configuration and Outputs

The simulations began on 1 August 1980 and ran through 31 July 2022. Temporal resolution was 3 h to capture diurnal variations, and the parcel-specific outputs (e.g. snow depth, snow density, and snow-ice thickness) were saved at the end of each day. Ice parcel trajectories were linearly interpolated from weekly to 3-hourly time steps. On 1 August of each year (except in the first year), the multi-year ice thicknesses were calculated from the sea ice thickness distribution on 31 July. The 1 August 1980 ice thickness initial condition was defined by performing a one-year simulation with a domain-wide initial condition of 1 m, and then using the ice thickness distribution at the end of the first simulation year as the initial condition for the beginning of the 42-year simulation (i.e., the model ran the first year twice and assumed the 31 July 1981 ice thickness distribution equaled the 1 August 1980 distribution). In addition, any snow remaining at 00:00 UTC on 1 August (the last time step on 31 July) was used as the initial condition for the following simulation year that started at 03:00 UTC on 1 August (these are the standard procedures implemented in Liston, Itkin, et al. (2020)).

The daily simulation outputs for each parcel (approximately 61,000 parcels each year) were gridded to the 25 km $\times$ 25 km Equal-Area Scalable Earth (EASE) grid, provided by NSIDC. The location of each parcel was used to calculate the overlap between that parcel and the EASE grid cell, i.e. the fractional area of the EASE grid cell that was occupied by the parcel. The fractional area was then multiplied by the sea ice concentration of the parcel, and the result was used to weigh the parcels' contribution to each EASE grid cell. This procedure of area- and concentration-weighted averages within the EASE grid cells conserved the examined parameters, similar to Merkouriadi et al. (2020).

2.6 Altimetry Applications

To study the impact of snow-ice formation in a wider context, we tested the SnowModel-LG_HS snow estimates in sea ice thickness retrievals from satellite altimetry. From the European Space Agency's (ESA) CryoSat-2 satellite, we processed Baseline-D (Baseline-E for winter 2021–2022) Level 1B Synthetic Aperture Radar (SAR) and SAR Interferometric files (European Space Agency, 2019a, 2019b, 2019c, 2019d) for the full winter season (September to May), starting in November 2010 and continuing through May 2022, using the python library pysiral (Hendricks et al., 2021). For the necessary auxiliary data in the sea ice thickness retrieval, we used the mean dynamic topography product by the Danish Technical University (DTU22MDT; Knudsen et al., 2022); for sea ice concentration and type, we used the European Organisation for the Exploitation of Meteorological Satellites (EUMETSAT) Ocean and Sea Ice Satellite Application Facility (OSI SAF) products 401-b and 403-d, respectively (OSI SAF, 2017a, 2017b).

The SnowModel-LG and SnowModel-LG_HS snow depths and densities were applied to preprocessed Level 1B files, and the processor was run first to produce Level 2 (along-track) and then to grid those to Level 3 (monthly gridded) files. For this study, we used the monthly gridded files.

2.7 Evaluation Exercise

To evaluate modeled snow depth and sea ice thickness, we compared them against independent airborne data from NASA OIB and Alfred Wegener Institute's (AWI) IceBird campaigns conducted during late-winter over the western Arctic. Snow depth data were derived from airborne snow radars similar on both OIB (99 flights in 2009–2019; Kurtz et al., 2015, 2016; MacGregor et al., 2021) and IceBird campaigns (11 flights in 2017 & 2019; Jutila et al., 2021a, 2021b; Jutila, King, et al., 2022), whereas sea ice thickness could be simultaneously and independently observed only on IceBird with a towed electromagnetic sounding instrument (Jutila et al., 2021a, 2021b; Jutila, Hendricks, et al., 2022). We averaged the airborne measurements over the same EASE grid when more than 50 values were present in a grid cell. For sea ice thickness, we included only level ice measurements using the flag in the data product that implements a total thickness gradient threshold of 4 cm within an along-track distance of 1 m.

In addition, we evaluated temperature profile and heating cycle data from thermistor strings of Snow Ice Mass Balance Apparatus (SIMBA) buoys (Jackson et al., 2013) deployed in the Arctic in 2012–2020 to detect flooding (Grosfeld et al., 2016; Lei et al., 2021, 2022, 2023). Changes in thermal diffusivity, temperature, and heat propagation distinguish the temporal evolution of different layers and their thicknesses (e.g. Provost et al., 2017).

3 Results

In this section, we present two snow depth and density products. The first product is based on the original SnowModel-LG model, without accounting for snow-ice formation. We refer to it as SMLG. SMLG is identical to the one described in Liston, Itkin, et al. (2020), only here the SnowModel-LG run was extended for four more years (1 August 1980 to 31 July 2022). The second product accounts for snow-ice formation through the coupling of SnowModel-LG with HIGHTSI (SnowModel-LG_HS). We refer to this simulation as SMLG_HS. In what follows, we compare snow depth and density derived by the two different products, and we use both to retrieve sea ice thickness from CryoSat-2.

The model results indicated that snow-ice has the potential to form every year in the Arctic Ocean, and it is characterized by strong seasonal and regional variations. The seasonality and long-term trends of snow-ice thickness calculated in this study were consistent with earlier findings (Merkouriadi et al., 2020), as expected. The seasonal and interannual evolution of all simulated parameters is presented in Figure S1. Our coupled SMLG_HS simulation presented herein investigated the impact of snow-ice formation on snow depth and density (Figures 1a–c and d–f, respectively). Snow-ice formation occurred throughout the 42-year simulation period (1980–2022), and it was more prominent in the Atlantic sector of the Arctic Ocean, north of Svalbard, across the east coast of Greenland, and over the Lincoln Sea. Here, we show results averaged across the 42-year period on the day of maximum snow-on-sea-ice volume.

The date of maximum snow-on-sea-ice volume occurred on average on 21 April with a standard deviation of 14 d. There was no significant long-term trend of that date across the simulation period. The snow depth and density differences (SMLG_HS minus SMLG) were calculated on the date of maximum snow volume and averaged over the 42-year period (e.g., Figures 1c and f). Across the Arctic Ocean, accounting for snow-ice formation produced a 20 % snow depth decrease and a 2 % snow density increase, corresponding to 4 cm of snow depth and 6.6 $\mathrm{kg\,m^{-3}}$ of snow density. Regional variations were strong, yielding over 85 cm decrease in snow depth, and 209 $\mathrm{kg\,m^{-3}}$ increase in snow density, when compared to the original SMLG product.

Sea ice thickness retrievals from CryoSat-2 were performed using both SMLG and SMLG_HS. Averaged results from April are plotted together with the differences in sea ice thickness in Figure 1g–i. SMLG_HS represents less snow load on sea ice, resulting in thinner sea ice thickness retrievals by 7.7 % (domain average) across the CryoSat-2 era (2011–2022). Even though there are regional and inter-annual variations, the differences were more prominent in the Atlantic sector of the Arctic Ocean and over the Lincoln Sea (Figure 1g–i), i.e. in regions that are more prone to snow-ice formation (Merkouriadi et al., 2020). The differences regionally exceed 1 m in April, highlighting the sensitivity of the altimetry retrievals to snow load.

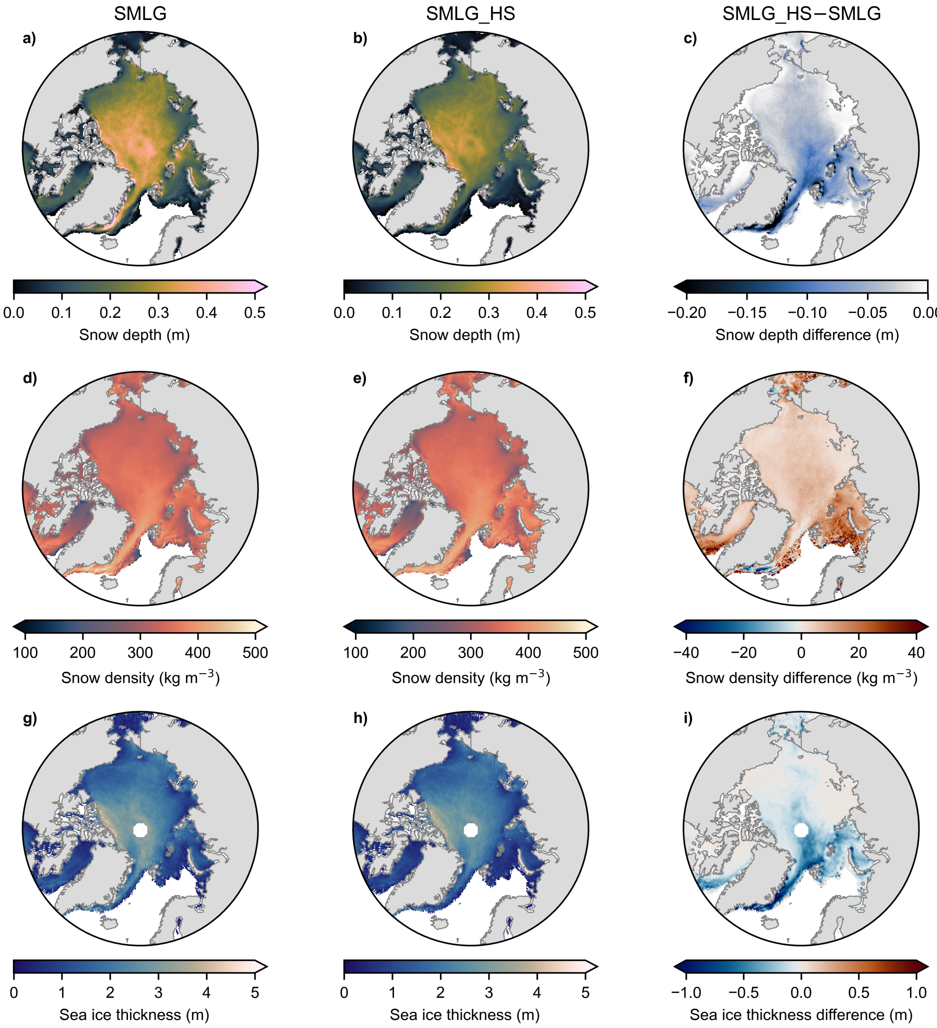

Figure 1. Snow depth (top) and snow density (middle) on the day of maximum snow-on-sea-ice volume (42-year average) as well as sea ice thickness (bottom) based on CryoSat-2 retrievals in April 2011–2022 from (a, d, g) SMLG, (b, e, h) SMLG_HS, and (c, f, i) the difference between the two products (SMLG_HS minus SMLG).

4 Discussion and Conclusions

We investigated the effect of snow-ice formation in snow depth and density reconstructions over Arctic sea ice in a modeling study. We did this by coupling SnowModel-LG snow depth and density evolution with HIGHTSI thermodynamic sea ice and snow-ice growth. When snow-ice was accounted for, snow depth decreased markedly and, in most cases, snow density increased. Averaged across the entire Arctic Ocean on the day of maximum snow-on-sea-ice volume, and for the period 1980–2022, snow depth given by SMLG_HS was 20 % lower than SMLG, and snow density was 2 % higher, corresponding to 4 cm of snow depth and 6.6 kg m^{-3} of snow density. Due to the large regional variations of snow-ice formation, snow depth decreased over 85 cm and density increased over 209 kg m^{-3} locally. The largest differences were found in the Atlantic sector of the Arctic Ocean, where snow-ice has the highest potential to form (Merkouriadi et al., 2020).

Largest differences in altimetry-derived sea ice thickness were found in the Atlantic sector and the Lincoln Sea, and they were consistent with the snow-ice contribution. In some years, the differences were notable in the central Arctic as well. Domain average sea ice thicknesses for the CryoSat-2 in April 2011–2022 were 7.7 % lower when using SMLG_HS compared to SMLG. It is worth mentioning that the effect of snow salinity on the altimetry signals becomes relevant when seawater floods the bottom of the snowpack (Willatt et al., 2010). SMLG_HS does not yet handle snow salinity and wicking in response to seawater flooding at the snow/ice interface. In addition to this, there is no temperature dependency in snow-ice formation in SMLG_HS. The model assumes that flooding — or negative freeboard — at the snow/ice interface corresponds to snow-ice formation in winter.

Due to the lack of information regarding several aspects of snow on sea ice, this study comes with some limitations. First, we assumed that a negative freeboard always results in snow-ice formation. In reality, for flooding to occur, water pathways such as sea ice thermal cracks or leads are required. Even though these pathways become increasingly common in a thinner and more dynamic icescape (Kwok et al., 2013; Rampal et al., 2009), our assumption likely resulted in overestimation of snow-ice formation. Second, we did not account for snow blowing into leads. Recent observations from the MOSAiC expedition demonstrated that this is likely an insignificant snow sink in winter, due to quick refreeze of the leads (Clemens-Sewall et al., 2023). This is further supported by the arguments put forth by Liston, Itkin, et al. (2020). Third, we assumed that snow accumulates on level ice, and we did not account for snow redistribution over deformed ice. Sea ice deformation features such as pressure ridges, are prominent in the Arctic Ocean, especially under a thinner and more dynamic sea ice regime (Itkin et al., 2017; Rampal et al., 2009). Snow tends to accumulate on the lee side of pressure ridges and other roughness elements (e.g. Liston et al., 2018), resulting in uneven snow load over a sea ice floe.

SMLG_HS snow depth fit well to both OIB and IceBird observations (Figures 2a–d), with reduced root-mean-square-errors and biases compared to SMLG (Figure S2). However, SMLG_HS constantly underestimated sea ice thickness of level ice, when compared to IceBird observations (Figures 2e–h and S3). We hypothesize that the sea ice thickness underestimation resulted from overestimation of the snow accumulation over level ice. Even though the total snow depth (over both deformed and level ice) matched well with the observations, not accounting for snow redistribution over deformed ice resulted in overestimation of snow depth over level ice. This additional snow decelerated thermodynamic ice growth, resulting in thinner sea ice that was more prone to snow-ice formation. Mid-winter flooding events at the snow/ice interface detected by IMBs supported our simulations of snow-ice formation (Figure S4). However, IMBs are point measurements and do not necessarily reflect the situation over larger spatial domains.

Although snow depth, and the associated snow-ice formation, have decreased Arctic-wide, modeling studies have indicated increasing trends in snow depth (Webster et al.,

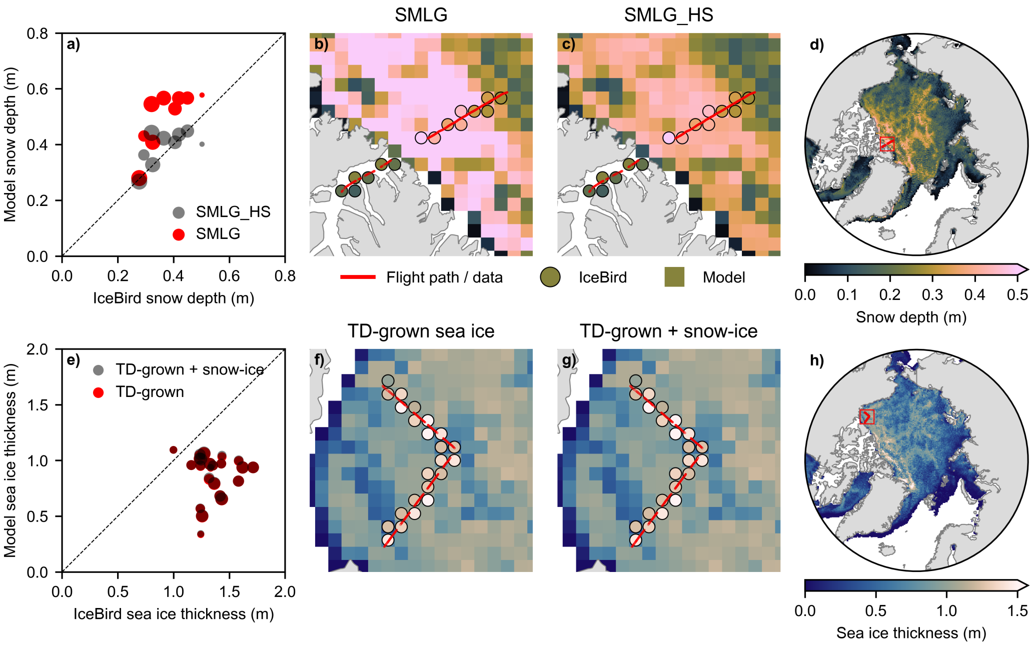

Figure 2. Panels a)–d) show the evaluation of modeled snow depth from SMLG and SMLG_HS against airborne radar-derived snow depth measurements from the AWI IceBird survey flight on 30 March 2017. Panels e)–h) show the evaluation of thermodynamically-grown (TD-grown) sea ice and snow-ice modeled with SMLG_HS against airborne sea ice thickness measurements over level ice from the AWI IceBird survey flight on 2 April 2017.

2019) and snow-ice (Merkouriadi et al., 2020) regionally in the Atlantic sector of the Arctic Ocean, especially along the east coast of Greenland, north of Svalbard, and at the Lincoln Sea since the 1980s. The increase is significant and it is associated with the intensification of storms that bring more precipitation to this part of the Arctic (Graham et al., 2017; Rinke et al., 2017; Woods & Caballero, 2016). When snow models do not account for snow sinks caused by snow and sea ice interactions, such as snow-ice formation or snow redistribution over sea ice deformation features, they overestimate snow depth on level ice. Uneven snow-on-sea-ice load within a sub-grid area will result in biases in altimetry retrievals of sea ice thickness by overestimating level ice and underestimating deformed ice thickness. Regarding sea ice modeling applications, spatial variability in snow depth will impact sea ice thermodynamic growth in winter and will affect meltpond formation in summer. Therefore, snow-on-sea-ice reconstructions should be used with caution depending on the application requirements. This study emphasizes the need to account for snow and sea ice interactions to improve the representation of snow on sea ice in both numerical modeling and remote sensing applications.

Data Availability Statement

Model input

Sea ice concentration data are available at DiGirolamo et al. (2022). Sea ice motion vectors are available at Tschudi et al. (2019). Atmospheric forcing data are available at Global Modeling And Assimilation Office (GMAO) (2015a, 2015b). Daily ocean heat flux data were downloaded from ECMWF.

Model output

Interannual variations of EASE-grid snow depth, snow density, and snow-ice thickness from 1 August 1980 through 31 July 2022 presented in this paper are available at Merkouriadi et al. (2023).

Altimetry input

CryoSat-2 Level 1B Baseline D/E SAR and SARIn data are available at European Space Agency (2019a, 2019b, 2019c, 2019d). Mean dynamic topography data are available at Knudsen et al. (2022). Sea ice concentration and type data are available at OSI SAF (2017a, 2017b), respectively. Python processing library pysiral is available at Hendricks et al. (2021).

Evaluation

Airborne data are available at Jutila et al. (2021a, 2021b); Jutila et al. (2021a, 2021b) for AWI IceBird and at Kurtz et al. (2015, 2016) for NASA OIB. SIMBA buoy data were obtained from `https://www.meereisportal.de` and Lei et al. (2021, 2022, 2023).

Acknowledgments

IM was supported by the ESA grant CCI+ 4000126449/19/I-NB. IM and AJ were supported by the Research Council of Finland grant 341550. GEL was supported by the United States National Science Foundation grant 1820927. AP was supported by the European Union's Horizon 2020 research and innovation programme under grant 101003472. The authors are grateful for Bin Cheng for providing the software code for the model HIGHTSI. Autonomous sea ice measurements (temperature profile and heating cycle data) from 2012 to 2020 were obtained from `https://www.meereisportal.de` (grant: REKLIM-2013-04). Scientific, colour-vision deficiency friendly, and perceptually-uniform color maps used in the figures of this manuscript were provided by Crameri (2023).

References

Blanchard-Wrigglesworth, E., Farrell, S. L., Newman, T., & Bitz, C. M. (2015). Snow cover on Arctic sea ice in observations and an Earth System Model. *Geophysical Research Letters*, *42*, 10,342–10,348. doi: 10.1002/2015GL066049

Blanchard-Wrigglesworth, E., Webster, M. A., Farrell, S. L., & Bitz, C. M. (2018). Reconstruction of Snow on Arctic Sea Ice. *Journal of Geophysical Research: Oceans*, *123*, 3588–3602. doi: 10.1002/2017JC013364

Briegleb, B., Bitz, C., Hunke, E., Lipscomb, W., Holland, M., Schramm, J., & Moritz, R. (2004). *Scientific Description of the Sea Ice Component in the Community Climate System Model, Version 3* (Tech. Rep.). University Corporation for Atmospheric Research. doi: 10.5065/D6HH6H1P

Cheng, B., Mäkynen, M., Similä, M., Rontu, L., & Vihma, T. (2013). Modelling snow and ice thickness in the coastal Kara Sea, Russian Arctic. *Annals of Glaciology*, *54*, 105–113. doi: 10.3189/2013AoG62A180

Cheng, B., Vihma, T., Zhanhai, Z., Zhijun, L., & Huiding, W. (2008). Snow and sea ice thermodynamics in the Arctic: Model validation and sensitivity study against SHEBA data. *Advances in Polar Science*, *19*, 108-122. Retrieved from `https://aps.chinare.org.cn/EN/Y2008/V19/I2/108`

Cheng, B., Zhang, Z., Vihma, T., Johansson, M., Bian, L., Li, Z., & Wu, H. (2008). Model experiments on snow and ice thermodynamics in the Arctic Ocean with CHINARE 2003 data. *Journal of Geophysical Research*, *113*, C09020. doi: 10.1029/2007JC004654

Clemens-Sewall, D., Polashenski, C., Frey, M. M., Cox, C. J., Granskog, M. A., Macfarlane, A. R., . . . Perovich, D. (2023). Snow Loss Into Leads in Arctic Sea Ice: Minimal in Typical Wintertime Conditions, but High During a Warm and Windy Snowfall Event. *Geophysical Research Letters*, *50*, e2023GL102816. doi: 10.1029/2023GL102816

Crameri, F. (2023). *Scientific colour maps.* Zenodo. doi: 10.5281/ZENODO.1243862

DiGirolamo, N., Parkinson, C., Cavalieri, D., Gloersen, P., & Zwally, H. (2022). *Sea Ice Concentrations from Nimbus-7 SMMR and DMSP SSM/I-SSMIS Passive Microwave Data, Version 2* [data set]. NASA National Snow and Ice Data Center Distributed Active Archive Center. (Accessed: 2 April 2023) doi: 10.5067/MPYG15WAA4WX

European Space Agency. (2019a). *L1b SARin Precise Orbit. Baseline D.* [data set]. (Accessed: 29 October 2023) doi: 10.5270/cr2-u3805kw

European Space Agency. (2019b). *L1b SARin Precise Orbit. Baseline E.* [data set]. (Accessed: 29 October 2023) doi: 10.5270/CR2-6afef01

European Space Agency. (2019c). *L1b SAR Precise Orbit. Baseline D.* [data set]. (Accessed: 29 October 2023) doi: 10.5270/cr2-2cnblvi

European Space Agency. (2019d). *L1b SAR Precise Orbit. Baseline E.* [data set]. (Accessed: 29 October 2023) doi: 10.5270/CR2-fbae3cd

Gelaro, R., McCarty, W., Suárez, M. J., Todling, R., Molod, A., Takacs, L., . . . Zhao, B. (2017). The Modern-Era Retrospective Analysis for Research and Applications, Version 2 (MERRA-2). *Journal of Climate*, *30*, 5419–5454. doi: 10.1175/JCLI-D-16-0758.1

Giles, K., Laxon, S., Wingham, D., Wallis, D., Krabill, W., Leuschen, C., . . . Raney, R. (2007). Combined airborne laser and radar altimeter measurements over the Fram Strait in May 2002. *Remote Sensing of Environment*, *111*, 182–194. doi: 10.1016/j.rse.2007.02.037

Global Modeling And Assimilation Office (GMAO). (2015a). *MERRA-2 tavg1_2d_flx_Nx: 2d, 1-Hourly, Time-Averaged, Single-Level, Assimilation, Surface Flux Diagnostics V5.12.4* [data set]. NASA Goddard Earth Sciences Data and Information Services Center. (Accessed: 7 January 2023) doi: 10.5067/7MCPBJ41Y0K6

Global Modeling And Assimilation Office (GMAO). (2015b). *MERRA-2 tavg1_2d_slv_Nx: 2d, 1-Hourly, Time-Averaged, Single-Level, Assimilation, Single-Level Diagnostics V5.12.4* [data set]. NASA Goddard Earth Sciences Data and Information Services Center. (Accessed: 7 January 2023) doi: 10.5067/VJAFPLI1CSIV

Graham, R. M., Rinke, A., Cohen, L., Hudson, S. R., Walden, V. P., Granskog, M. A., . . . Maturilli, M. (2017). A comparison of the two Arctic atmospheric winter states observed during N-ICE2015 and SHEBA. *Journal of Geophysical Research: Atmospheres*, *122*, 5716–5737. doi: 10.1002/2016JD025475

Granskog, M. A., Rösel, A., Dodd, P. A., Divine, D., Gerland, S., Martma, T., & Leng, M. J. (2017). Snow contribution to first-year and second-year Arctic sea ice mass balance north of Svalbard. *Journal of Geophysical Research: Oceans*, *122*, 2539–2549. doi: 10.1002/2016JC012398

Grenfell, T. C., & Maykut, G. A. (1977). The Optical Properties of Ice and Snow in the Arctic Basin. *Journal of Glaciology*, *18*, 445–463. doi: 10.3189/S0022143000021122

Grosfeld, K., Treffeisen, R., Asseng, J., Bartsch, A., Bräuer, B., Fritzsch, B., . . . Weigelt, M. (2016). Online Sea-Ice Knowledge and Data Platform. *Polarforschung; 85*. doi: 10.2312/POLFOR.2016.011

Hendricks, S., Sallila, H., Brockley, D., & Paul, S. (2021). *shendric/pysiral: Product update (C3S, AWI, CCI, CryoTEMPO)* [software]. Zenodo. (Accessed: 29 October 2023) doi: 10.5281/zenodo.5566347

Hersbach, H., Bell, B., Berrisford, P., Hirahara, S., Horányi, A., Muñoz-Sabater, J.,

… Thépaut, J. (2020). The ERA5 global reanalysis. *Quarterly Journal of the Royal Meteorological Society*, *146*, 1999–2049. doi: 10.1002/qj.3803

Itkin, P., Spreen, G., Cheng, B., Doble, M., Girard-Ardhuin, F., Haapala, J., … Wilkinson, J. (2017). Thin ice and storms: Sea ice deformation from buoy arrays deployed during N-ICE2015. *Journal of Geophysical Research: Oceans*, *122*, 4661–4674. doi: 10.1002/2016JC012403

Jackson, K., Wilkinson, J., Maksym, T., Meldrum, D., Beckers, J., Haas, C., & Mackenzie, D. (2013). A novel and low-cost sea ice mass balance buoy. *Journal of Atmospheric and Oceanic Technology*, *30*, 2676-2688. doi: 10.1175/JTECH-D-13-00058.1

Jutila, A., Hendricks, S., Ricker, R., von Albedyll, L., & Haas, C. (2021a). *Airborne sea ice parameters during the IceBird Winter 2019 campaign in the Arctic Ocean, version 1* [data set]. PANGAEA. (Accessed: 18 July 2023) doi: 10.1594/PANGAEA.933912

Jutila, A., Hendricks, S., Ricker, R., von Albedyll, L., & Haas, C. (2021b). *Airborne sea ice parameters during the PAMARCMIP2017 campaign in the Arctic Ocean, version 1* [data set]. PANGAEA. (Accessed: 18 July 2023) doi: 10.1594/PANGAEA.933883

Jutila, A., Hendricks, S., Ricker, R., von Albedyll, L., Krumpen, T., & Haas, C. (2022). Retrieval and parameterisation of sea-ice bulk density from airborne multi-sensor measurements. *The Cryosphere*, *16*, 259-275. doi: 10.5194/tc-16-259-2022

Jutila, A., King, J., Paden, J., Ricker, R., Hendricks, S., Polashenski, C., … Haas, C. (2022). High-Resolution Snow Depth on Arctic Sea Ice From Low-Altitude Airborne Microwave Radar Data. *IEEE Transactions on Geoscience and Remote Sensing*, *60*, 1-16. doi: 10.1109/TGRS.2021.3063756

Jutila, A., King, J., Ricker, R., Hendricks, S., Helm, V., Binder, T., & Haas, C. (2021a). *Airborne snow depth on sea ice during the IceBird Winter 2019 campaign in the Arctic Ocean, Version 1.* PANGAEA. (Accessed: 18 July 2023) doi: 10.1594/PANGAEA.932790

Jutila, A., King, J., Ricker, R., Hendricks, S., Helm, V., Binder, T., & Herber, A. (2021b). *Airborne snow depth on sea ice during the PAMARCMIP2017 campaign in the Arctic Ocean, Version 1.* PANGAEA. (Accessed: 18 July 2023) doi: 10.1594/PANGAEA.932668

Knudsen, P., Andersen, O., Maximenko, N., & Hafne, J. (2022). *A new combined mean dynamic topography model — DTUUH22MDT* [data set]. Retrieved from `https://ftp.spacecenter.dk/pub/DTU22/MDT/` (Accessed: 29 October 2023)

Kurtz, N. T., Markus, T., Cavalieri, D. J., Sparling, L. C., Krabill, W. B., Gasiewski, A. J., & Sonntag, J. G. (2009). Estimation of sea ice thickness distributions through the combination of snow depth and satellite laser altimetry data. *Journal of Geophysical Research*, *114*, C10007. doi: 10.1029/2009JC005292

Kurtz, N. T., Studinger, M., Harbeck, J., DePaul Onana, V., & Yi, D. (2015). *IceBridge L4 Sea Ice Freeboard, Snow Depth, and Thickness, Version 1.* NASA National Snow and Ice Data Center Distributed Active Archive Center. (Accessed: 18 July 2023) doi: 10.5067/G519SHCKWQV6

Kurtz, N. T., Studinger, M., Harbeck, J., DePaul Onana, V., & Yi, D. (2016). *IceBridge Sea Ice Freeboard, Snow Depth, and Thickness Quick Look, Version 1.* NASA National Snow and Ice Data Center Distributed Active Archive Center. Retrieved from `https://nsidc.org/data/NSIDC-0708/versions/1` (Accessed: 18 July 2023) doi: 10.5067/GRIXZ91DE0L9

Kwok, R., & Cunningham, G. F. (2008). ICESat over Arctic sea ice: Estimation of snow depth and ice thickness. *Journal of Geophysical Research*, *113*, C08010. doi: 10.1029/2008JC004753

Kwok, R., Cunningham, G. F., Wensnahan, M., Rigor, I., Zwally, H. J., & Yi, D. (2009). Thinning and volume loss of the Arctic Ocean sea ice cover: 2003–2008. *Journal of Geophysical Research*, *114*, C07005. doi: 10.1029/2009JC005312

Kwok, R., Spreen, G., & Pang, S. (2013). Arctic sea ice circulation and drift speed: Decadal trends and ocean currents. *Journal of Geophysical Research: Oceans*, *118*, 2408–2425. doi: 10.1002/jgrc.20191

Landy, J. C., Dawson, G. J., Tsamados, M., Bushuk, M., Stroeve, J. C., Howell, S. E. L., … Aksenov, Y. (2022). A year-round satellite sea-ice thickness record from CryoSat-2. *Nature*, *609*(7927), 517–522. doi: 10.1038/s41586-022-05058-5

Landy, J. C., Petty, A. A., Tsamados, M., & Stroeve, J. C. (2020). Sea Ice Roughness Overlooked as a Key Source of Uncertainty in CryoSat-2 Ice Freeboard Retrievals. *Journal of Geophysical Research: Oceans*, *125*, e2019JC015820. doi: 10.1029/2019JC015820

Launiainen, J., & Cheng, B. (1998). Modelling of ice thermodynamics in natural water bodies. *Cold Regions Science and Technology*, *27*, 153–178. doi: 10.1016/S0165-232X(98)00009-3

Laxon, S., Peacock, N., & Smith, D. (2003). High interannual variability of sea ice thickness in the Arctic region. *Nature*, *425*, 947–950. doi: 10.1038/nature02050

Lei, R., Cheng, B., Hoppmann, M., Nicolaus, M., & Regnery, J. (2023). *Temperature and heating induced temperature difference measurements from SIMBA-type sea ice mass balance buoy 2020T84, deployed during MOSAiC 2020/21* [data set]. PANGAEA. (Accessed: 6 September 2023) doi: 10.1594/PANGAEA.958397

Lei, R., Cheng, B., Hoppmann, M., & Zuo, G. (2021). *Temperature and heating induced temperature difference measurements from SIMBA-type sea ice mass balance buoy 2019T69, deployed during MOSAiC 2019/20* [data set]. PANGAEA. (Accessed: 6 September 2023) doi: 10.1594/PANGAEA.938096

Lei, R., Cheng, B., Hoppmann, M., & Zuo, G. (2022). *Temperature and heating induced temperature difference measurements from SIMBA-type sea ice mass balance buoy 2019T72, deployed during MOSAiC 2019/20* [data set]. PANGAEA. (Accessed: 6 September 2023) doi: 10.1594/PANGAEA.940668

Leppäranta, M. (1983). A Growth Model for Black Ice, Snow Ice and Snow Thickness in Subarctic Basins. *Hydrology Research*, *14*, 59–70. doi: 10.2166/nh.1983.0006

Liston, G. E., & Elder, K. (2006a). A Distributed Snow-Evolution Modeling System (SnowModel). *Journal of Hydrometeorology*, *7*, 1259–1276. doi: 10.1175/JHM548.1

Liston, G. E., & Elder, K. (2006b). A Meteorological Distribution System for High-Resolution Terrestrial Modeling (MicroMet). *Journal of Hydrometeorology*, *7*(2), 217–234. doi: 10.1175/JHM486.1

Liston, G. E., Itkin, P., Stroeve, J., Tschudi, M., Stewart, J. S., Pedersen, S. H., … Elder, K. (2020). A Lagrangian Snow-Evolution System for Sea-Ice Applications (SnowModel-LG): Part I — Model Description. *Journal of Geophysical Research: Oceans*, *125*, e2019JC015913. doi: 10.1029/2019JC015913

Liston, G. E., Polashenski, C., Rösel, A., Itkin, P., King, J., Merkouriadi, I., & Haapala, J. (2018). A Distributed Snow-Evolution Model for Sea-Ice Applications (SnowModel). *Journal of Geophysical Research: Oceans*, *123*, 3786–3810. doi: 10.1002/2017JC013706

Liston, G. E., Stroeve, J., & Itkin, P. (2020). *Lagrangian Snow Distributions for Sea-Ice Applications* [data set]. NASA National Snow and Ice Data Center Distributed Active Archive Center. doi: 10.5067/27A0P5M6LZBI

Macfarlane, A. R., Schneebeli, M., Dadic, R., Tavri, A., Immerz, A., Polashenski, C., ... Fons, S. (2023). A Database of Snow on Sea Ice in the Central Arctic Collected during the MOSAiC expedition. *Scientific Data*, *10*, 398. doi: 10.1038/s41597-023-02273-1

MacGregor, J. A., Boisvert, L. N., Medley, B., Petty, A. A., Harbeck, J. P., Bell, R. E., ... Yungel, J. K. (2021). The Scientific Legacy of NASA's Operation IceBridge. *Reviews of Geophysics*, *59*. doi: 10.1029/2020RG000712

Markus, T., Neumann, T., Martino, A., Abdalati, W., Brunt, K., Csatho, B., ... Zwally, J. (2017). The Ice, Cloud, and land Elevation Satellite-2 (ICESat-2): Science requirements, concept, and implementation. *Remote Sensing of Environment*, *190*, 260–273. doi: 10.1016/j.rse.2016.12.029

Maslanik, J. A., Fowler, C., Stroeve, J., Drobot, S., Zwally, J., Yi, D., & Emery, W. (2007). A younger, thinner Arctic ice cover: Increased potential for rapid, extensive sea-ice loss. *Geophysical Research Letters*, *34*, L24501. doi: 10.1029/2007GL032043

Maykut, G. A., & Untersteiner, N. (1971). Some results from a time-dependent thermodynamic model of sea ice. *Journal of Geophysical Research*, *76*, 1550–1575. doi: 10.1029/JC076i006p01550

Meier, W. N., Hovelsrud, G. K., van Oort, B. E., Key, J. R., Kovacs, K. M., Michel, C., ... Reist, J. D. (2014). Arctic sea ice in transformation: A review of recent observed changes and impacts on biology and human activity. *Reviews of Geophysics*, *52*, 185–217. doi: 10.1002/2013RG000431

Merkouriadi, I., Cheng, B., Graham, R. M., Rösel, A., & Granskog, M. A. (2017). Critical Role of Snow on Sea Ice Growth in the Atlantic Sector of the Arctic Ocean. *Geophysical Research Letters*, *44*, 10,479–10,485. doi: 10.1002/2017GL075494

Merkouriadi, I., Liston, G. E., Graham, R. M., & Granskog, M. A. (2020). Quantifying the Potential for Snow-Ice Formation in the Arctic Ocean. *Geophysical Research Letters*, *47*, e2019GL085020. doi: 10.1029/2019GL085020

Merkouriadi, I., Liston, G. E., & Jutila, A. (2023). *Investigating the effect of snow-ice formation on snow depth and density over Arctic sea ice* [data set]. Finnish Meteorological Institute. doi: 10.57707/fmi-b2share.529adcd77c144d82a7b29841e34922a3

OSI SAF. (2017a). *Global Sea Ice Concentration (netCDF) - DMSP* [data set]. OSI SAF. (Accessed: 29 October 2023) doi: 10.15770/EUM_SAF_OSI_NRT_2004

OSI SAF. (2017b). *Global Sea Ice Type (netCDF) - Multimission* [data set]. OSI SAF. (Accessed: 29 October 2023) doi: 10.15770/EUM_SAF_OSI_NRT_2006

Perovich, D. K. (1996). *The optical properties of sea ice* (Tech. Rep.). Cold Regions Research and Engineering Laboratory. Retrieved from `http://hdl.handle.net/11681/2648`

Petty, A. A., Webster, M., Boisvert, L., & Markus, T. (2018). The NASA Eulerian Snow on Sea Ice Model (NESOSIM) v1.0: initial model development and analysis. *Geoscientific Model Development*, *11*, 4577–4602. doi: 10.5194/gmd-11-4577-2018

Pringle, D. J., Eicken, H., Trodahl, H. J., & Backstrom, L. G. E. (2007). Thermal conductivity of landfast Antarctic and Arctic sea ice. *Journal of Geophysical Research*, *112*, C04017. doi: 10.1029/2006JC003641

Provost, C., Sennéchael, N., Miguet, J., Itkin, P., Rösel, A., Koenig, Z., ... Granskog, M. A. (2017). Observations of flooding and snow-ice formation in a thinner Arctic sea-ice regime during the N-ICE 2015 campaign: Influence of basal ice melt and storms. *Journal of Geophysical Research: Oceans*, *122*, 7115–7134. doi: 10.1002/2016JC012011

Rampal, P., Weiss, J., & Marsan, D. (2009). Positive trend in the mean speed and deformation rate of Arctic sea ice, 1979–2007. *Journal of Geophysical Research*, *114*, C05013. doi: 10.1029/2008JC005066

Rinke, A., Maturilli, M., Graham, R. M., Matthes, H., Handorf, D., Cohen, L.,

… Moore, J. C. (2017). Extreme cyclone events in the Arctic: Wintertime variability and trends. *Environmental Research Letters*, *12*, 094006. doi: 10.1088/1748-9326/aa7def

Saloranta, T. M. (2000). Modeling the evolution of snow, snow ice and ice in the Baltic Sea. *Tellus A: Dynamic Meteorology and Oceanography*, *52*, 93. doi: 10.3402/tellusa.v52i1.12255

Stroeve, J. C., Liston, G. E., Buzzard, S., Zhou, L., Mallett, R., Barrett, A., … Stewart, J. S. (2020). A Lagrangian Snow Evolution System for Sea Ice Applications (SnowModel-LG): Part II — Analyses. *Journal of Geophysical Research: Oceans*, *125*, e2019JC015900. doi: 10.1029/2019JC015900

Stroeve, J. C., Markus, T., Boisvert, L., Miller, J., & Barrett, A. (2014). Changes in Arctic melt season and implications for sea ice loss. *Geophysical Research Letters*, *41*, 1216–1225. doi: 10.1002/2013GL058951

Tschudi, M., Meier, W. N., & Stewart, J. S. (2020). An enhancement to sea ice motion and age products at the National Snow and Ice Data Center (NSIDC). *The Cryosphere*, *14*(5), 1519–1536. doi: 10.5194/tc-14-1519-2020

Tschudi, M., Meier, W. N., Stewart, J. S., Fowler, C., & Maslanik, J. (2019). *Polar Pathfinder Daily 25 km EASE-Grid Sea Ice Motion Vectors, Version 4* [data set]. NASA National Snow and Ice Data Center Distributed Active Archive Center. (Accessed: 20 March 2023) doi: 10.5067/INAWUWO7QH7B

Wang, C., Cheng, B., Wang, K., Gerland, S., & Pavlova, O. (2015). Modelling snow ice and superimposed ice on landfast sea ice in Kongsfjorden, Svalbard. *Polar Research*, *34*, 20828. doi: 10.3402/polar.v34.20828

Warren, S. G., Rigor, I. G., Untersteiner, N., Radionov, V. F., Bryazgin, N. N., Aleksandrov, Y. I., & Colony, R. (1999). Snow Depth on Arctic Sea Ice. *Journal of Climate*, *12*, 1814–1829. doi: 10.1175/1520-0442(1999)012⟨1814:SDOASI⟩2.0.CO;2

Webster, M. A., Parker, C., Boisvert, L., & Kwok, R. (2019). The role of cyclone activity in snow accumulation on Arctic sea ice. *Nature Communications*, *10*, 5285. doi: 10.1038/s41467-019-13299-8

Webster, M. A., Rigor, I. G., Nghiem, S. V., Kurtz, N. T., Farrell, S. L., Perovich, D. K., & Sturm, M. (2014). Interdecadal changes in snow depth on Arctic sea ice. *Journal of Geophysical Research: Oceans*, *119*, 5395–5406. doi: 10.1002/2014JC009985

Willatt, R., Giles, K., Laxon, S., Stone-Drake, L., & Worby, A. (2010). Field Investigations of Ku-Band Radar Penetration Into Snow Cover on Antarctic Sea Ice. *IEEE Transactions on Geoscience and Remote Sensing*, *48*, 365–372. doi: 10.1109/TGRS.2009.2028237

Woods, C., & Caballero, R. (2016). The Role of Moist Intrusions in Winter Arctic Warming and Sea Ice Decline. *Journal of Climate*, *29*, 4473–4485. doi: 10.1175/JCLI-D-15-0773.1

Zuo, H., Balmaseda, M. A., Tietsche, S., Mogensen, K., & Mayer, M. (2019). The ECMWF operational ensemble reanalysis–analysis system for ocean and sea ice: a description of the system and assessment. *Ocean Science*, *15*(3), 779–808. doi: 10.5194/os-15-779-2019

Zygmuntowska, M., Rampal, P., Ivanova, N., & Smedsrud, L. H. (2014). Uncertainties in Arctic sea ice thickness and volume: new estimates and implications for trends. *The Cryosphere*, *8*, 705–720. doi: 10.5194/tc-8-705-2014

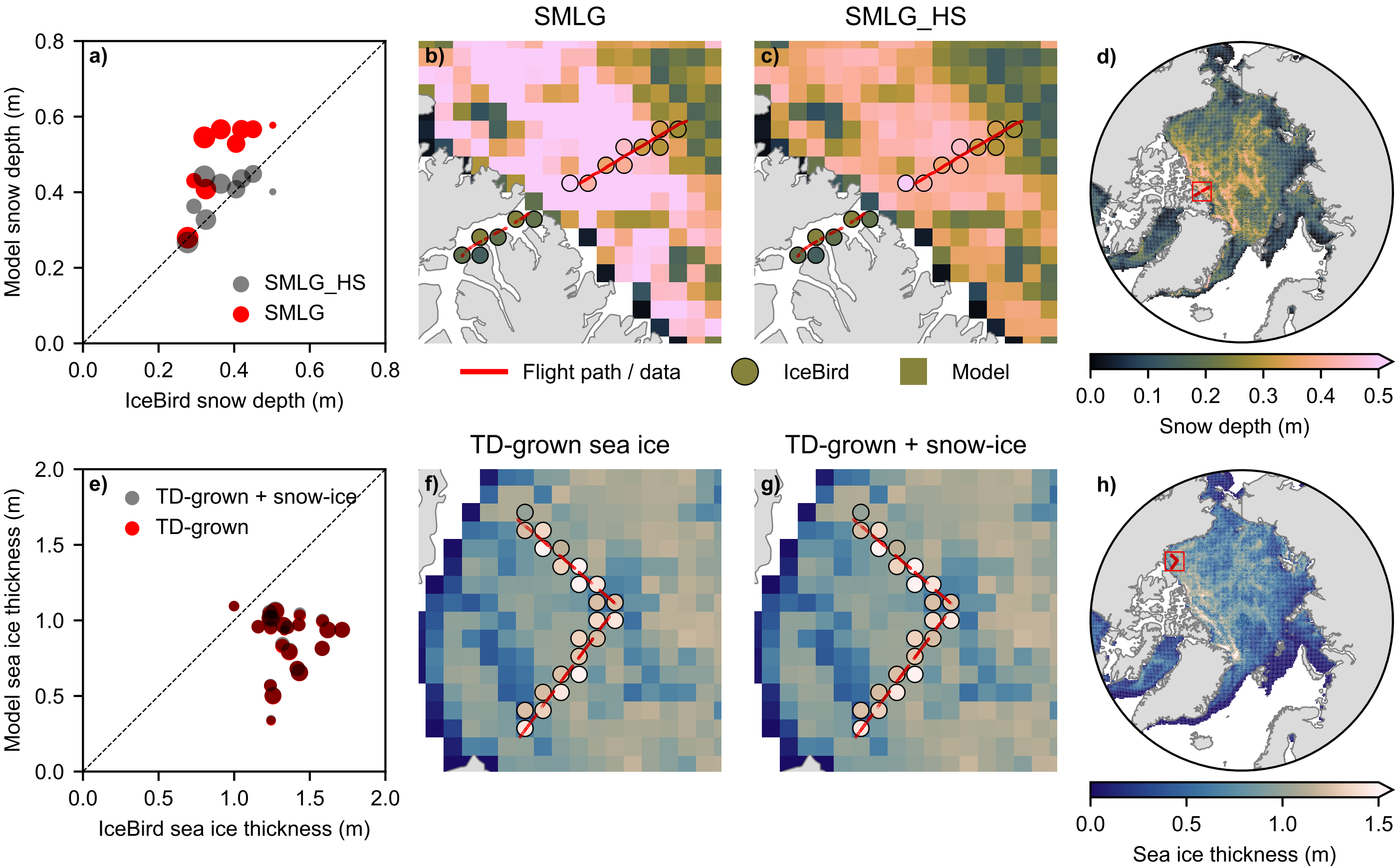

SMLG
SMLG_HS
a)
b)
c)
d)
Model snow depth (m)
IceBird snow depth (m)
SMLG_HS
SMLG
Flight path / data
IceBird
Model
Snow depth (m)
TD-grown sea ice
TD-grown + snow-ice
e)
f)
g)
h)
TD-grown + snow-ice
TD-grown
Model sea ice thickness (m)
IceBird sea ice thickness (m)
Sea ice thickness (m)

Supporting Information for “Investigating the Effect of Snow-Ice Formation on Snow Depth and Density over Arctic Sea Ice”

I. Merkouriadi[1], G. E. Liston[2], A. Jutila[1], H. Sallila[1], A. Preußer[3]

[1]Finnish Meteorological Institute, Helsinki, Finland

[2]Cooperative Institute for Research in the Atmosphere, Colorado State University, Fort Collins, CO, USA

[3]Alfred-Wegener-Institut, Helmholtz-Zentrum für Polar- und Meeresforschung, Bremerhaven, Germany

Contents of this file

Introduction

The supporting information includes three short supporting texts (S1–S3) explaining one table (S1) and four figures (S1–S4).

Corresponding author: I. Merkouriadi, Finnish Meteorological Institute, Helsinki, Finland. (ioanna.merkouriadi@fmi.fi)

Text S1. Model parametrization. Table S1 is descriptive, and it includes the HIGHTSI model parameterization used in this study.

Text S2. Seasonality. Figure S1 shows the seasonal cycle of the modeled parameters over 42 years. While snow, snow-ice, thermodynamically-grown sea ice, and total sea ice are expressed in pan-Arctic volume (m^3), snow density is the pan-Arctic average ($kg\,m^{-3}$).

Text S3. Evaluation exercise. Figure S2 shows the results of the evaluation exercise, where we compared modeled snow depth against gridded airborne radar-derived snow depth measurements from the NASA Operation IceBridge campaigns in 2009–2019 and the Alfred Wegener Institute's (AWI) IceBird campaigns in 2017 & 2019.

Figure S3 shows the comparison of modeled sea ice thickness against airborne sea ice thickness measurements over level ice from the AWI IceBird campaigns. Smaller values of RMSE and mean bias in 2017 than in 2019 are due to the fact that the AWI IceBird airborne surveys in 2017 covered only first-year ice.

Figure S4 shows a summary of the data from the Snow Ice Mass Balance Apparatus (SIMBA) buoys, where we identified wintertime formation of snow-ice. The height of the snow/ice interface shows a shift upward together with a decrease in snow depth at the presence of modeled snow-ice formation.

References

Briegleb, B., Bitz, C., Hunke, E., Lipscomb, W., Holland, M., Schramm, J., & Moritz, R. (2004). *Scientific Description of the Sea Ice Component in the Community Climate System Model, Version 3* (Tech. Rep.). University Corporation for Atmospheric Research. doi: 10.5065/D6HH6H1P

Cheng, B., Vihma, T., Zhanhai, Z., Zhijun, L., & Huiding, W. (2008). Snow and sea ice thermodynamics in the Arctic: Model validation and sensitivity study against SHEBA data. *Advances in Polar Science*, *19*, 108-122. Retrieved from https://aps.chinare.org.cn/EN/Y2008/V19/I2/108

Granskog, M. A., Rösel, A., Dodd, P. A., Divine, D., Gerland, S., Martma, T., & Leng, M. J. (2017). Snow contribution to first-year and second-year Arctic sea ice mass balance north of Svalbard. *Journal of Geophysical Research: Oceans*, *122*, 2539–2549. doi: 10.1002/2016JC012398

Grenfell, T. C., & Maykut, G. A. (1977). The Optical Properties of Ice and Snow in the Arctic Basin. *Journal of Glaciology*, *18*, 445–463. doi: 10.3189/S0022143000021122

Liston, G. E., Itkin, P., Stroeve, J., Tschudi, M., Stewart, J. S., Pedersen, S. H., ... Elder, K. (2020). A Lagrangian Snow-Evolution System for Sea-Ice Applications (SnowModel-LG): Part I — Model Description. *Journal of Geophysical Research: Oceans*, *125*, e2019JC015913. doi: 10.1029/2019JC015913

Maykut, G. A., & Untersteiner, N. (1971). Some results from a time-dependent thermodynamic model of sea ice. *Journal of Geophysical Research*, *76*, 1550–1575. doi: 10.1029/JC076i006p01550

Perovich, D. K. (1996). *The optical properties of sea ice* (Tech. Rep.). Cold Regions Research and Engineering Laboratory. Retrieved from http://hdl.handle.net/11681/2648

Pringle, D. J., Eicken, H., Trodahl, H. J., & Backstrom, L. G. E. (2007). Thermal conductivity of landfast Antarctic and Arctic sea ice. *Journal of Geophysical Research*, *112*, C04017. doi: 10.1029/2006JC003641

Wang, C., Cheng, B., Wang, K., Gerland, S., & Pavlova, O. (2015). Modelling snow ice and superimposed ice on landfast sea ice in Kongsfjorden, Svalbard. *Polar Research*, *34*, 20828. doi: 10.3402/polar.v34.20828

Zuo, H., Balmaseda, M. A., Tietsche, S., Mogensen, K., & Mayer, M. (2019). The ECMWF operational ensemble reanalysis–analysis system for ocean and sea ice: a description of the system and assessment. *Ocean Science*, *15*(3), 779–808. doi: 10.5194/os-15-779-2019

Table S1. Model parameters and constants used in this study.

Parameter	**Value**	**Remarks/Source**
Extinction coefficient of sea ice (k_i)	1.5–$17\,\mathrm{m}^{-1}$	adopted from the paper by Grenfell and Maykut (1977)
Extinction coefficient of snow (k_s)	15–$25\,\mathrm{m}^{-1}$	Perovich (1996)
Surface albedo ($\alpha_{s,i}$)	Time dependent	Briegleb et al. (2004)
Freezing point (T_f)	$-1.8\,°\mathrm{C}$	
Sea ice volumetric heat capacity (ρc_i)	Function of T_i, s_i	Maykut and Untersteiner (1971)
Heat capacity of ice (c_i)	$2{,}093\,\mathrm{J\,kg^{-1}\,K^{-1}}$	
Latent heat of freezing (L_i)	$0.33 \times 10^6\,\mathrm{J\,kg^{-1}}$	
Oceanic heat flux (F_w)	Time dependent	ECMWF; Zuo, Balmaseda, Tietsche, Mogensen, and Mayer (2019)
Sea ice density (ρ_i)	$910\,\mathrm{kg\,m^{-3}}$	
Snow-ice density (ρ_{si})	$850\,\mathrm{kg\,m^{-3}}$	Wang, Cheng, Wang, Gerland, and Pavlova (2015)
Slush density (ρ_{sl})	$920\,\mathrm{kg\,m^{-3}}$	Wang et al. (2015)
Sea ice salinity (s_i)	1–6	Ice core measurement Granskog et al. (2017)
Snow density (ρ_s)	Time dependent	Liston et al. (2020)
Surface emissivity (e)	0.97	
Sea ice heat conductivity (k_{si})	Function of T_i, s_i	Pringle, Eicken, Trodahl, and Backstrom (2007)
Thermal conductivity of ice (k_i)	$2.03\,\mathrm{W\,m^{-2}}$	Maykut and Untersteiner (1971)
Time step of model (t)	3 h	
Initial temperature in snow and ice	$[-1.25\,°\mathrm{C},\ -1.8\,°\mathrm{C}]$	Cheng, Vihma, Zhanhai, Zhijun, and Huiding (2008)
Number of layers in the ice	20	
Number of layers in the snow	25	

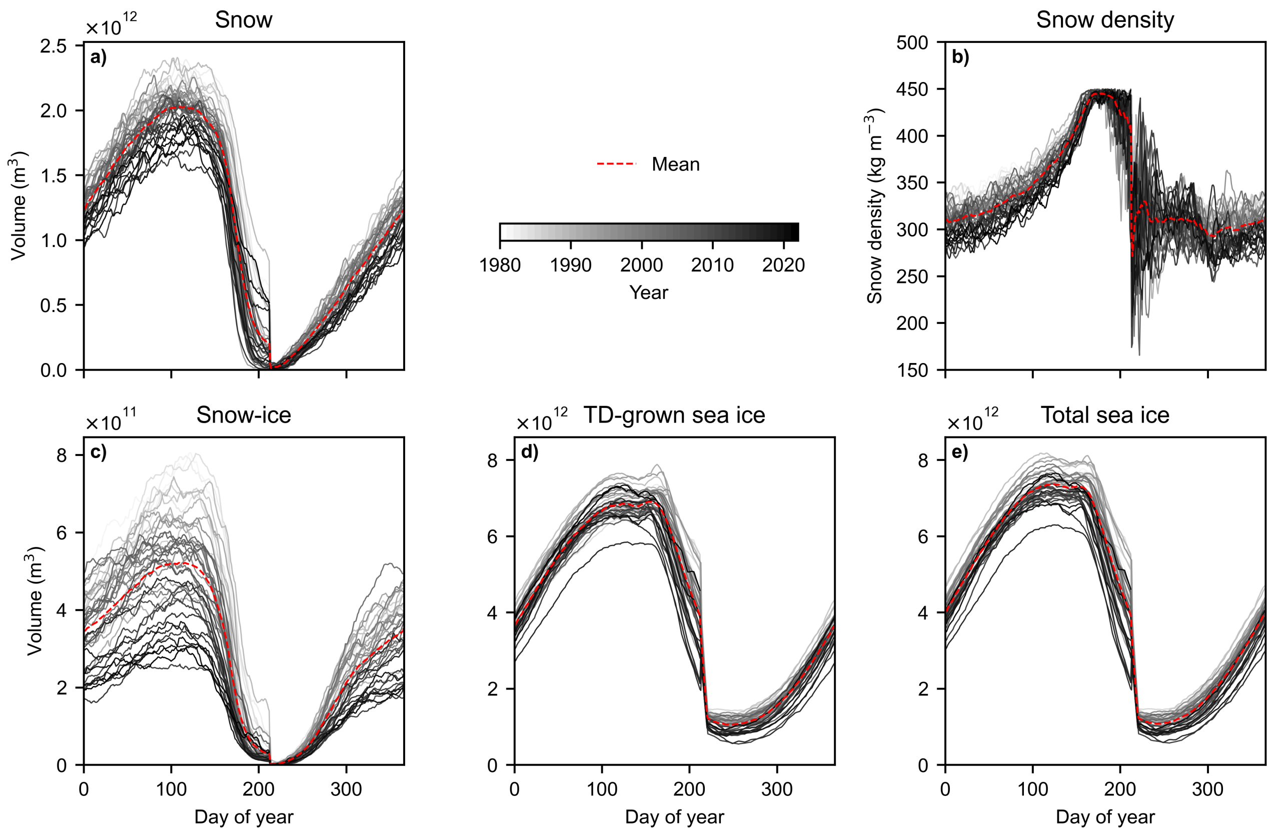

Figure S1. Seasonal cycle of the modeled parameters: a) snow, b) snow density, c) snow-ice, d) thermodynamically-grown (TD-grown) sea ice, and e) total sea ice. They are expressed in volume summed over the Arctic (note the varying scale of the vertical axes), except for snow density in panel b), which is a pan-Arctic average. Each individual greyscale line shows the daily evolution through the year for each of the 42 simulated years, while the red dashed line shows the mean of those 42 years.

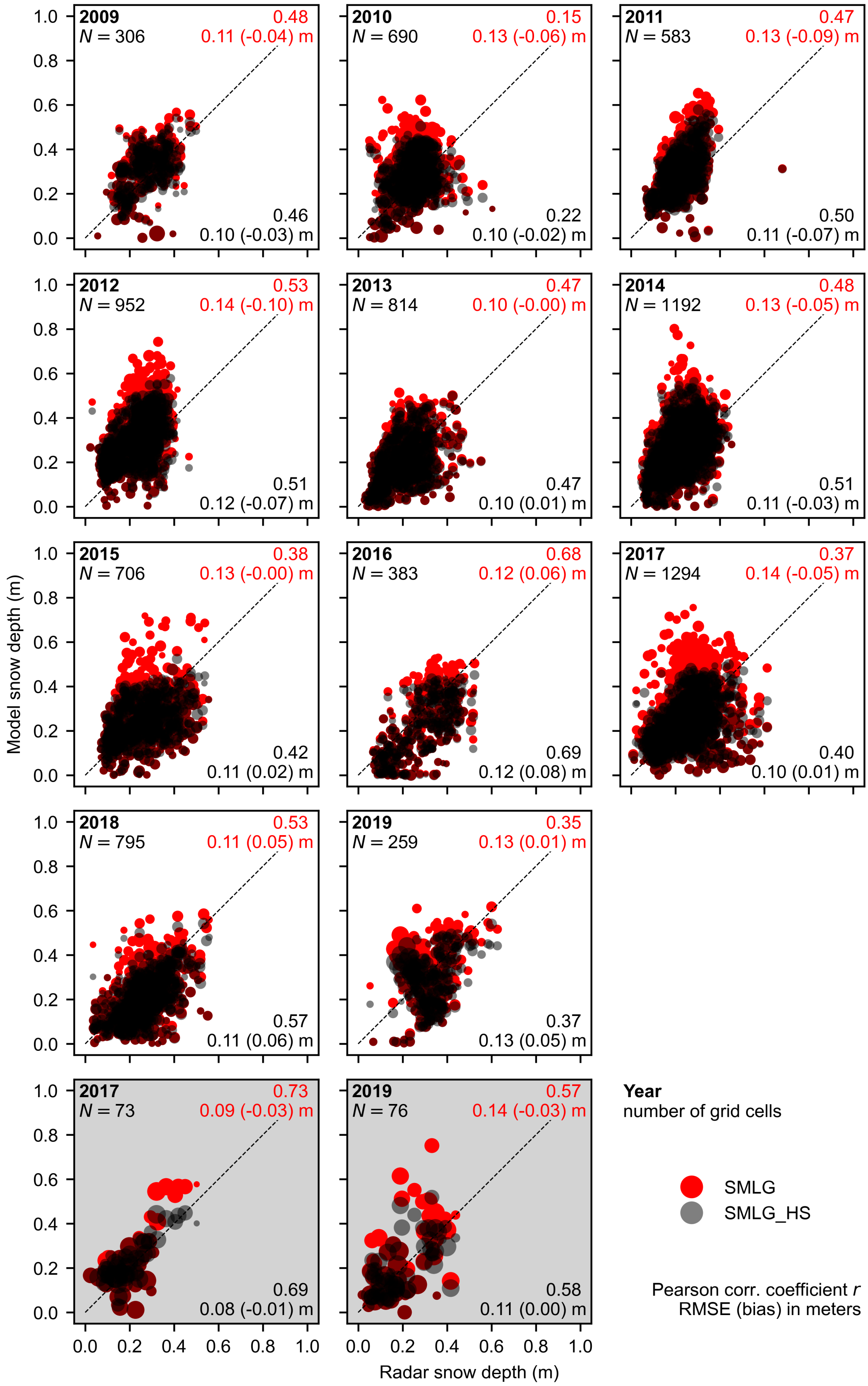
2009
N = 306
0.48
0.11 (-0.04) m
0.46
0.10 (-0.03) m
2010
N = 690
0.15
0.13 (-0.06) m
0.22
0.10 (-0.02) m
2011
N = 583
0.47
0.13 (-0.09) m
0.50
0.11 (-0.07) m
2012
N = 952
0.53
0.14 (-0.10) m
0.51
0.12 (-0.07) m
2013
N = 814
0.47
0.10 (-0.00) m
0.47
0.10 (0.01) m
2014
N = 1192
0.48
0.13 (-0.05) m
0.51
0.11 (-0.03) m
2015
N = 706
0.38
0.13 (-0.00) m
0.42
0.11 (0.02) m
2016
N = 383
0.68
0.12 (0.06) m
0.69
0.12 (0.08) m
2017
N = 1294
0.37
0.14 (-0.05) m
0.40
0.10 (0.01) m
2018
N = 795
0.53
0.11 (0.05) m
0.57
0.11 (0.06) m
2019
N = 259
0.35
0.13 (0.01) m
0.37
0.13 (0.05) m
2017
N = 73
0.73
0.09 (-0.03) m
0.69
0.08 (-0.01) m
2019
N = 76
0.57
0.14 (-0.03) m
0.58
0.11 (0.00) m
Model snow depth (m)
Radar snow depth (m)
Year
number of grid cells
SMLG
SMLG_HS
Pearson corr. coefficient r
RMSE (bias) in meters

Figure S2. Evaluation of the modeled snow depth, compared against gridded airborne radar-derived snow depth measurements. Panels with white background show the NASA Operation IceBridge campaigns in 2009–2019 and the bottom panels with grey background show the AWI IceBird campaigns in 2017 & 2019. Red color refers to the original SnowModel-LG and black color to the new, coupled SnowModel-LG_HS. The size of the data point reflects the relative number of airborne measurements in the grid cell. Upper and lower right corners of each panel show the statistics of the corresponding year: Pearson correlation coefficient r, root-mean-square error (RMSE), and lastly mean bias in parenthesis.

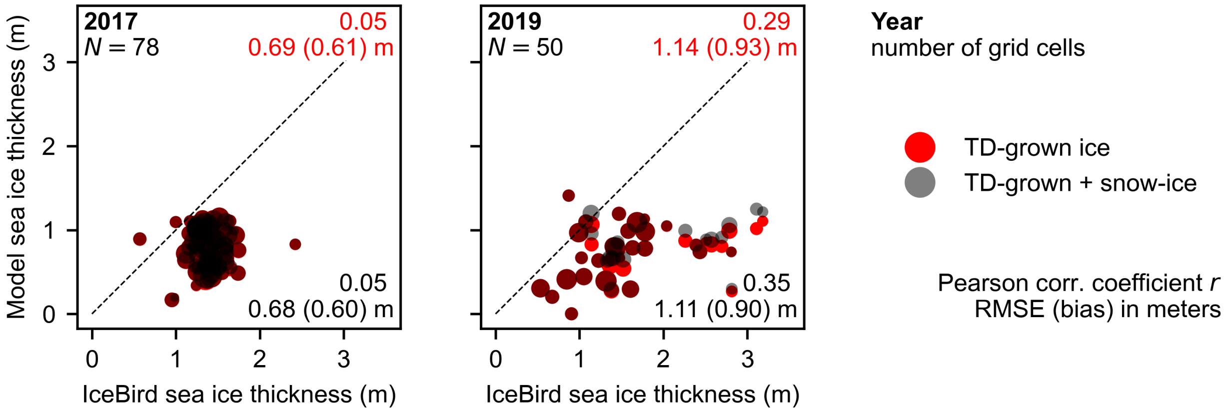

Figure S3. Evaluation of the modeled sea ice thickness, compared against gridded airborne sea ice thickness measurements over level ice from the AWI IceBird campaigns in 2017 & 2019. Red color refers to only thermodynamically-grown (TD-grown) sea ice, black color indicates the sum of TD-grown sea ice and snow-ice, i.e. total sea ice thickness. The size of the data point reflects the relative number of airborne measurements in the grid cell. Upper and lower right corners of each panel show the statistics of the corresponding year: Pearson correlation coefficient r, root-mean-square error (RMSE), and lastly mean bias in parenthesis.

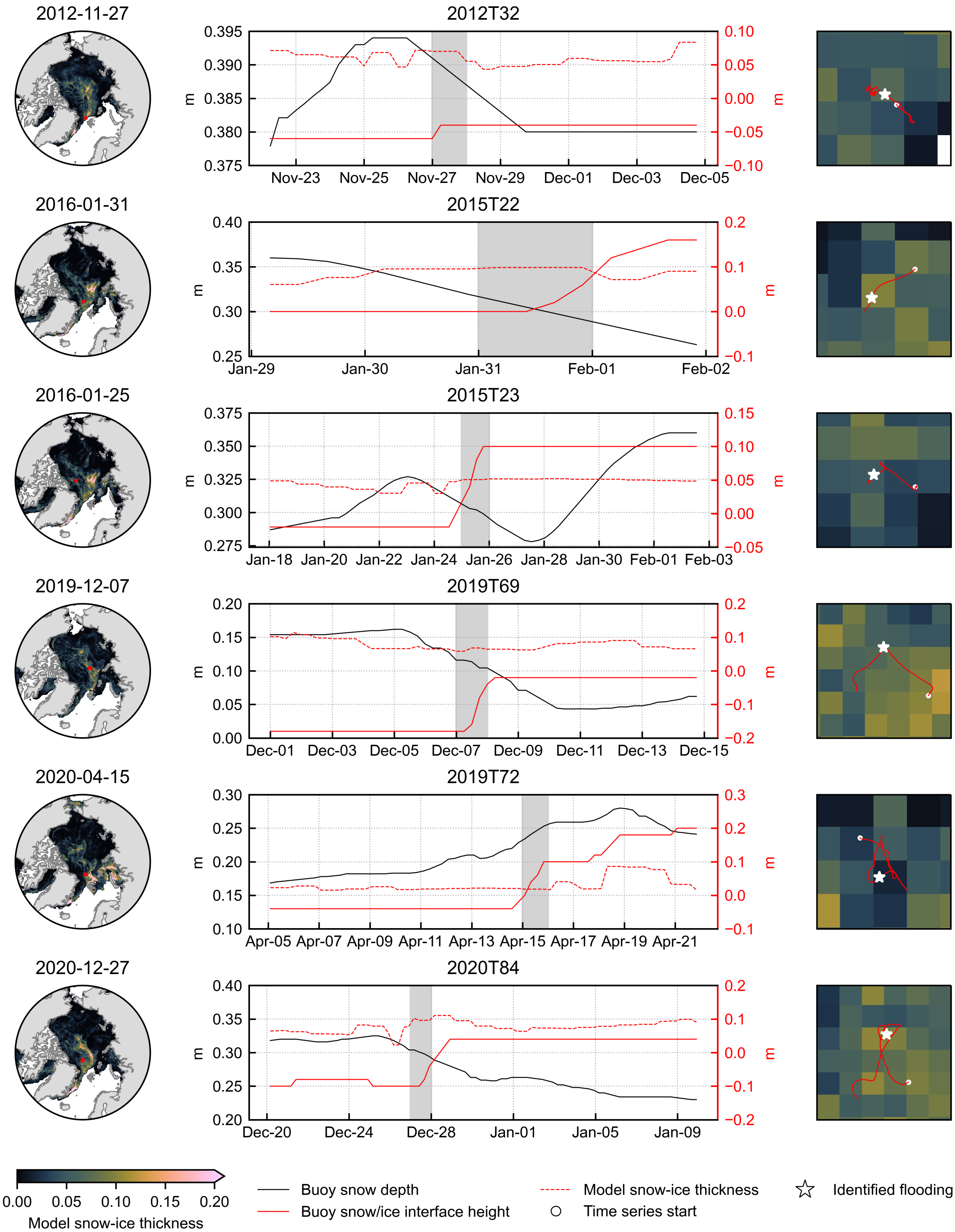
2012-11-27
2012T32
Nov-23 Nov-25 Nov-27 Nov-29 Dec-01 Dec-03 Dec-05
2016-01-31
2015T22
Jan-29 Jan-30 Jan-31 Feb-01 Feb-02
2016-01-25
2015T23
Jan-18 Jan-20 Jan-22 Jan-24 Jan-26 Jan-28 Jan-30 Feb-01 Feb-03
2019-12-07
2019T69
Dec-01 Dec-03 Dec-05 Dec-07 Dec-09 Dec-11 Dec-13 Dec-15
2020-04-15
2019T72
Apr-05 Apr-07 Apr-09 Apr-11 Apr-13 Apr-15 Apr-17 Apr-19 Apr-21
2020-12-27
2020T84
Dec-20 Dec-24 Dec-28 Jan-01 Jan-05 Jan-09
m
0.00 0.05 0.10 0.15 0.20
Model snow-ice thickness
Buoy snow depth
Buoy snow/ice interface height
Model snow-ice thickness
Time series start
Identified flooding

Figure S4. Evaluation of the snow-ice formation using Snow Ice Mass Balance Apparatus (SIMBA) buoys. The left panels show the pan-Arctic simulated snow-ice thickness with the buoy location marked with a red dot on the day of identified flooding events. The middle panels show the time series of the snow depth measured by the buoy (black solid line, left vertical axes), of the snow/ice interface height derived from the buoy data (red solid line, right vertical axes), and of the modeled snow-ice thickness of the nearest grid cell (red dashed line, right vertical axes) around the time of identified flooding events. The buoy names are given as the titles. Note the varying scales of the axes, both left and right vertical axes as well as the horizontal time axes. The gray background indicates the day depicted in the maps. The right panels show the drift track of the buoys with the start of the middle panel time series marked with a white dot and the time of identified flooding with a white star. Note the varying scale: however, a single grid cell is always 25 km $\times$ 25 km.

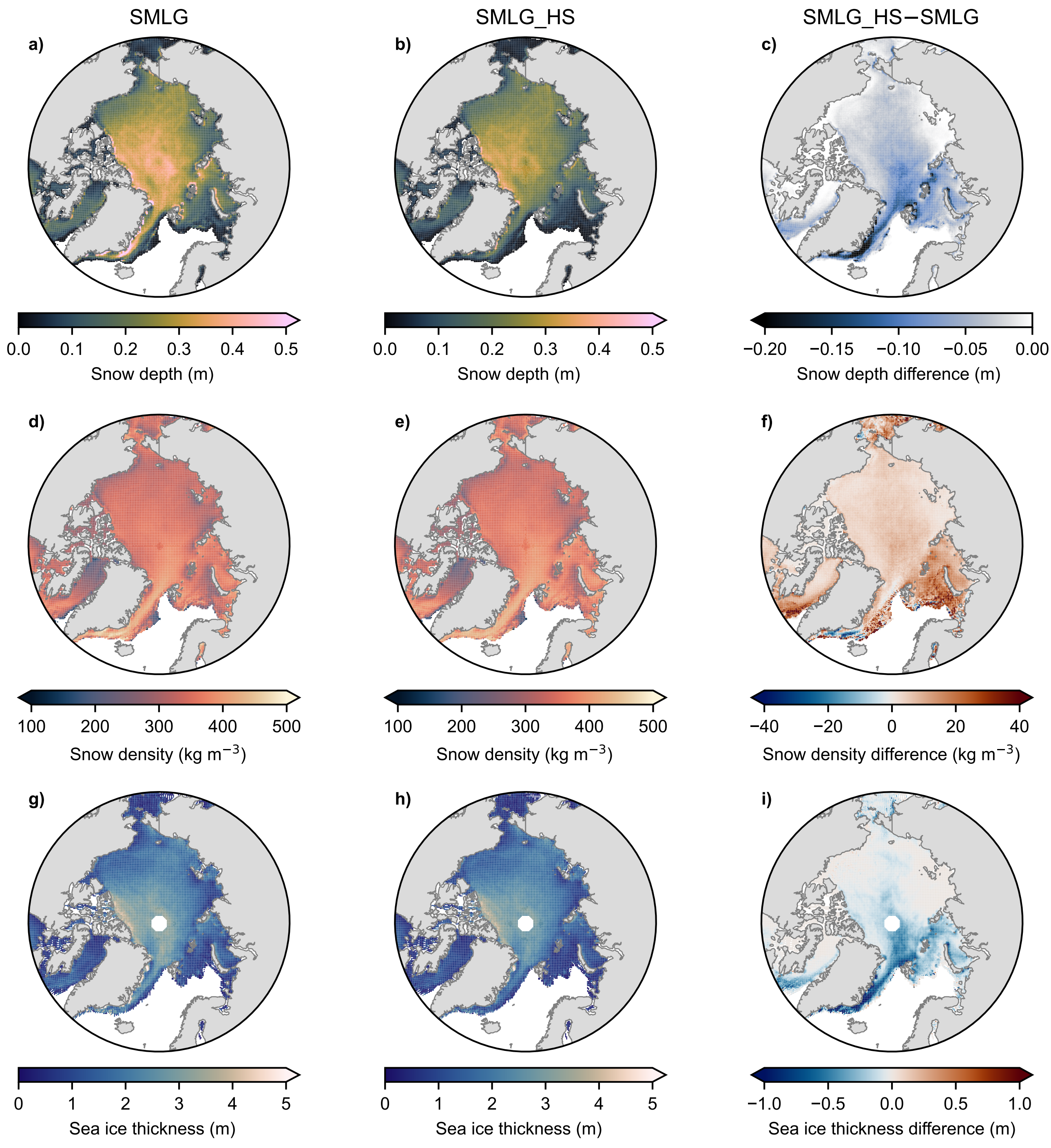
SMLG
SMLG_HS
SMLG_HS−SMLG
a)
b)
c)
0.0 0.1 0.2 0.3 0.4 0.5
Snow depth (m)
0.0 0.1 0.2 0.3 0.4 0.5
Snow depth (m)
−0.20 −0.15 −0.10 −0.05 0.00
Snow depth difference (m)
d)
e)
f)
100 200 300 400 500
Snow density (kg m−3)
100 200 300 400 500
Snow density (kg m−3)
−40 −20 0 20 40
Snow density difference (kg m−3)
g)
h)
i)
0 1 2 3 4 5
Sea ice thickness (m)
0 1 2 3 4 5
Sea ice thickness (m)
−1.0 −0.5 0.0 0.5 1.0
Sea ice thickness difference (m)